Multicritical behavior of Abrikosov vortex lattices near the cholesteric–smectic-A–smectic-C^* point

S. R. Renn
Laboratory of Atomic and Solid State Physics, Cornell University, Ithaca, New York 14853
(Received 7 June 1991)

The mean-field phase diagram of the cholesteric–smectic-A–smectic-C* (N^*–Sm-A–Sm-C^*) point is derived within the framework of the chiral Chen-Lubensky model. We show that on the Sm-C^* side of the phase diagram, one or two additional twist-grain-boundary (TGB) (or chiral-smectic) phases will occur. These additional chiral-smectic phases, the TGB_C and TGB_{C^*} phases, are highly dislocated versions of smectic-C and smectic-C^* phases, respectively. According to the de Gennes superconductor analogy, the grain-boundary phase which occurred on the smectic-A side of the phase diagram (known as the TGB_A or chiral Sm-A^*) is the analog of the Abrikosov vortex lattice in type-II superconductors. However, the TGB_C and TGB_{C^*} phases would correspond to Abrikosov vortex lattices in a hypothetical superconductor where the Ginzburg parameter κ is negative and the photon has Bose condensed. These additional phases are predicted to occur near the recently observed N^*–Sm-A^*–Sm-C^* multicritical point. We discuss the N^*-TGB_C, TGB_A-TGB_C, and TGB_A-TGB_{C^*} phase transitions. Because of the twist, the XY-like Sm-A–Sm-C is (usually) replaced by the Ising-like TGB_A-TGB_C. However, if the Sm-C^* helicoidal pitch length is somewhat smaller than the cholesteric pitch length, then the TGB_A-TGB_C transition would be replaced by the TGB_A-TGB_{C^*} transition.

PACS number(s): 61.30.Jf, 64.70.Md

I. INTRODUCTION

In the last two years there has been an effort by several groups [1–5] to understand the effect of chirality on smectic-A (Sm-A) liquid crystals. This work began with two independent and nearly simultaneous events: One was the prediction, by Renn and Lubensky [4], that chiral smectics could exhibit a new highly dislocated Sm-A phase called the twist-grain-boundary (TGB) phase. The basis for this prediction was the de Gennes model [6] which established a strong analogy (see Table I) between the nematic (N) to Sm-A transition and the normal-to-superconducting transition in metals. According to this analogy, a transition between the cholesteric (N^*) and Sm-A phases would occur either directly or would proceed through an intermediate phase characterized by a twisted lattice of screw dislocations (see Fig. 1). This intermediate phase was, in fact, the analog of Abrikosov's triangular flux vortex lattice [7,8] which occurs in type-II superconductors in an externally imposed magnetic field. Like Abrikosov's flux lattice, the TGB would occur if $\kappa \equiv \lambda/\xi$, the ratio of the twist penetration depth divided by the smectic coherence length, exceeded $1/\sqrt{2}$.

The other important development was the discovery, by Goodby *et al.* [1], of an experimental candidate, the Sm-A^* phase, first identified in the highly chiral homologous series S-1-methylheptyl 4′-[(4″-n-alkoxyphenyl) proppionoyloxyl-biphenyl-4-carboxylate] (nP1M7), with $n=13,14,15$. Because x-ray studies on nonaligned samples together with textural studies indicated that the Sm-A^* simultaneously exhibited both smectic layering and cholestericlike textures, Goodby *et al.* proposed that the

TABLE I. The de Gennes analogy between smectic-A liquid crystals and type-II superconductors.

Superconductor	Liquid crystal
ψ=Cooper pair amplitude	ψ=density-wave amplitude
$\mathbf{A}$=vector potential	$\hat{\mathbf{n}}$=nematic director
$\mathbf{B}=\nabla\times\mathbf{A}$=magnetic induction	$k_0\equiv\hat{\mathbf{n}}\cdot\nabla\times\hat{\mathbf{n}}$=twist
Normal metal	Nematic phase
Normal metal in a magnetic field	Cholesteric (N^*) phase
Meissner phase	Smectic-A phase
Meissner effect	Twist expulsion
London penetration depth, λ	Twist penetration depth, λ_2
Superconducting coherence length, ξ	Smectic correlation length ξ
Vortex (magnetic flux tube)	Screw dislocation
Abrikosov flux lattice	Twist-grain-boundary (TGB) phase

Sm-A^* might, in fact, be the TGB phase. This identification has since been confirmed by a high-resolution x-ray study on aligned samples by Srajer *et al.* [2]. The Srajer *et al.* study indicated that the Sm-A^* exhibited many features expected for the TGB phase. In particular, they found (1) long-range (>5000 Å) Sm-A correlations in the plane perpendicular to the pitch axis, (2) smectic-layer normals uniformly distributed in the plane perpendicular to the pitch axis, and (3) short-range (185-Å) smectic correlations along the pitch axis with a Gaussian wave-vector dependence. All these observations are consistent with a twisted stack of two-dimensional Sm-A slabs where the smectic order parameter of a slab is a Landau-orbit solution of the linearized Ginzburg-Landau–de Gennes equations.

The excitement of these discoveries has been further heightened by the recent discovery by Slaney and Goodby [9] of five new homogeneous series exhibiting the Sm-A^* phase. In several of these candidate materials, including nP1M7 (see Fig. 2) the Sm-A^* phase is observed to occur near a Sm-A–Sm-C^* phase boundary [10]. This, we believe, is quite significant. To understand why, we first recall that Abrikosov phases, such as the TGB, occur only when the ratio of the twist penetration depth λ_2 to the smectic coherence length ξ is large. This result together with the divergence of $\kappa \equiv \lambda_2/\xi$ at the Sm-A–Sm-C phase boundary makes the appearance of the TGB in materials like nP1M7 quite understandable [11].

In several of the compounds and mixtures exhibiting the Sm-A^* phase, one can infer the existence of a Sm-A–Sm-A^*–Sm-C^* multicritical point. These systems include mixtures of (15P1M7) and (9O2C14M5) mixtures [12,9] as well as levo and dextro nP1M7 mixtures [13]. In view of the existence of such multicritical points one might ask whether the TGB phase obtained by entering from the Sm-C^* side is the same phase obtained by entering the Sm-A side. In particular, one might expect [14] that entry from the Sm-C^* side gives rise to a new TGB phase consisting of Sm-C^* (or perhaps Sm-C) like slabs. One of the purposes of this paper is to investigate this possibility.

In addition, we would also like to take advantage of some unusual opportunities presented by the Sm-A–Sm-A^*–Sm-C^* point. In particular, it offers one an opportunity to understand (1) how the Abrikosov flux-dislocation lattice behaves when κ diverges (i.e., in the ex-

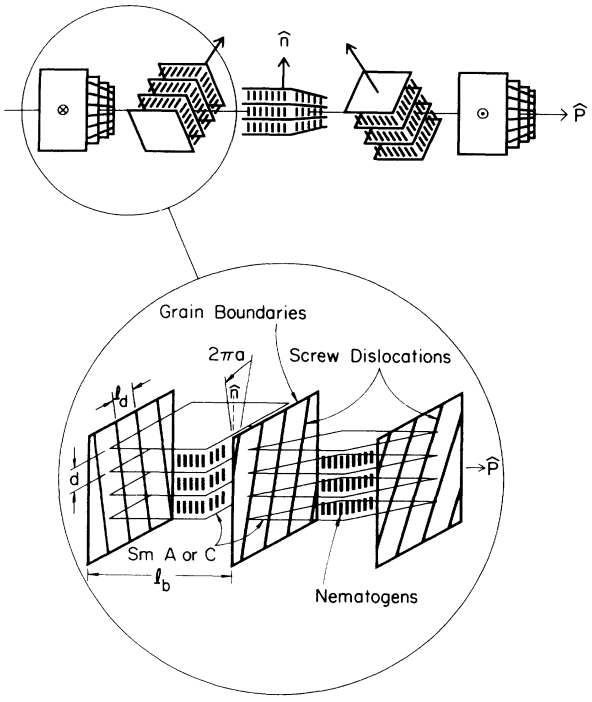

FIG. 1. The twist-grain-boundary (TGB_A or TGB_C) phases consist of a twisted array of infinite two-dimensional smectic slabs which are stacked along the pitch axis $\hat{\mathbf{P}}$. In the inset we see that between every pair of slabs there exists a grid of parallel equispaced screw dislocations. These grids are known as grain boundaries and, like the smectic slabs, also form a twisted stack. The TGB phases are characterized by a nonvanishing twist and long-range smectic correlations within the plane perpendicular to the pitch axis. According to the de Gennes superconductor analogy, the TGB_A is the analog of the Abrikosov vortex lattice where the screw dislocation lines correspond to magnetic flux vortices.

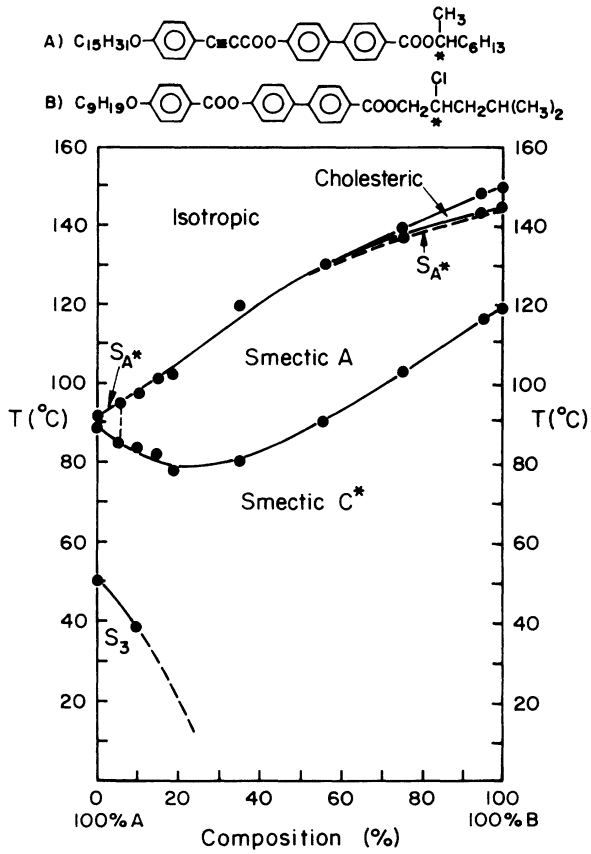

FIG. 2. Phase diagram of binary mixtures of 15P1M7 and 9O2C14M5. These two compounds, respectively labeled A and B, exhibit two distinct regions where the Sm-A^* phase is observed. For nearly pure 15P1M7 mixtures, one may infer a Sm-A^*–Sm-A–Sm-C^* multicritical point. The figure is courtesy of J. Goodby and A. Slaney. See Ref. [12].

treme type-II limit) and (2) how it behaves when the Meissner (twist expulsion) effect breaks down (e.g., when the Sm-C side of the phase diagram is entered). In a previous paper [5], we addressed the first question by examining the approach to the Sm-A–Sm-C boundary within the framework of the Chen-Lubensky model of the chiral N-A-C point. In this paper, we will continue our study of the chiral Chen-Lubensky model in order to address the second question.

We will find several remarkable features of the Sm-A–Sm-A^*–Sm-C^* multicritical point. The first is that one indeed finds new TGB phases here. In addition it provides a fascinating example of multicritical phenomenon involving Abrikosov vortex lattices. Finally, the transition between (commensurate) TGB_A and TGB_C phases may be the first theoretically described structural phase transition occurring in a system with quasicrystalline symmetry (see Appendix A and Ref. [15]).

We should pause to explain why one should study a model of the chiral N^*-A-C^* point to understand the nature of the Sm-A–Sm-A^*–Sm-C^* point. Indeed many of the smectics exhibiting the Sm-A^* phase often do not have a cholesteric (N^*) phase nearby. There are several reasons for using an N^*-A-C^*–point model. The first is that the chiral Chen-Lubensky [16] model of the chiral N^*-A-C^* point provides a relatively tractable example of a Sm-A–Sm-A^*–Sm-C^* point. In particular, the presence of weak smectic ordering, near a continuous N^* to TGB transition, will enable us to study phase transitions between different TGB phases in ways which, otherwise, would not be possible. The second reason is that one needs a theory of the Sm-A–Sm-C^* transition generalized in such a way as to describe the effect of a high density of dislocations. Of course, at sufficiently high dislocation densities (i.e., deep in the Sm-A^* phase, well away from the Sm-A–Sm-A^* transition) the dislocation cores will overlap. The smectic order is then destroyed, leaving only a uniformly twisted cholesteric. For this reason, the cholesteric phase is a natural part of the phase diagram. Moreover, as the chirality is turned off, the natural phase diagram reduces to an N-A-C point. This does not mean, of course, that the cholesteric phase is necessarily accessible in any given physical system.

As a result of this study, we will find that two additional TGB phases may occur on the Sm-C side of the phase diagram. Like the original TGB phase (the TGB_A), these additional TGB phases (the TGB_C and TGB_{C^*}) consist of a twisted array of two-dimensional smectic slabs, stacked along the pitch axis. The three phases are distinguished by the nature of the slabs: TGB_A, TGB_C, and TGB_{C^*} consist of Sm-A, Sm-C, and Sm-C^* slabs, respectively.

The other principle results of our analysis of the chiral N^*-A-C^* point are as follows. First we find that, with decreasing temperature, the N^*-TGB_C transition as well as the N^*-TGB_A can occur. In addition, we find that chirality will cause the Sm-A–Sm-C transition, near the N-A-C point, to be replaced by a TGB_A-TGB_C transition and (if $K_1 > K_3$ and $K_2 > K_3$) a TGB_A-TGB_{C^*} transition as well. We will also show that the TGB_A-TGB_C, according to mean-field theory, is a continuous Ising-like transition. Finally, we will discuss the several unusual multicritical points including, of course, the Sm-A–TGB_A–Sm-C^* point. These results, together with those previously obtained for the Sm-A side, are shown later in the mean-field chiral Chen-Lubensky phase diagram (see Figs. 11–13).

The organization of the paper is as follows. In Sec. II we reintroduce the chiral Chen-Lubensky model (first considered in Ref. [16]) and briefly summarize the results obtained there. In Sec. III we consider the instability of the cholesteric phase with respect to the development of Sm-C slabs. This instability demonstrates the formation of the TGB_C phase at a temperature T_{c2}. In Sec. IV we first discuss Sm-C^* dislocations and grain boundaries. Then we will introduce the structure of the TGB_{C^*} phase. In Sec. V we discuss the phase transitions between the TGB phases. It consists of three subsections. In Sec. V A we consider the point-group symmetries of the TGB_A and TGB_C phases. In Sec. V B we will derive a simplified stability operator which describes the mean-field TGB_A-TGB_C transition on length scales much larger than the grain-boundary spacing. In Sec. V C we will use it to analyze the TGB_A-TGB_C and TGB_A-TGB_{C^*} transitions. Finally in Sec. VI we summarize our results and make a few concluding remarks regarding some simple characteristics that should aid in the experimental identification of the new TGB phases. This paper also has two appendixes. In Appendix A we discuss some group theoretical issues that are raised by the TGB_A–TGB_C transition. In particular, we show that the spontaneous macroscopic symmetry breaking at the TGB_A to TGB_C transition will allow a second-order TGB_A-TGB_C transition even in the absence of a broken local symmetry. We will also give a symmetry classification of the possible TGB_A-TGB_C order parameters. In Appendix B we discuss the mean-field equation of state (i.e., twist versus chirality) of the TGB_A phase.

II. CHIRAL CHEN-LUBENSKY MODEL

The Chen-Lubensky (CL) model has been successful in explaining the experimental observations [17] of the N-A-C multicritical point. This model assumes that the x-ray scattering intensity in the nematic phase are spots along the director axis, if near the N–Sm-A transition, or diffuse rings centered along the same axis, if near the N–Sm-C transition. In the first half of this section, we will reintroduce a covariant version of this model, which we believe contains the essential physics needed to describe the effects of chirality on the N-A-C point. In particular, the covariant CL model reduces to the chiral and covariant de Gennes model first used to study the TGB_A phase. In addition, it clearly demonstrates how Sm-A changes from a type-I superconductor analog to a type-II analog as the Sm-A–Sm-C boundary is approached. Much is known from earlier studies about the Sm-A side of the CL phase diagram. So we will review some of the basic results [4,5,16] of these studies in the second half of

this section.

The covariant CL model may defined in terms of $\hat{n}$, the Frank director and ψ, the smectic order parameter. The latter is related to the molecular density $\rho(\mathbf{r})$, according to

$$\rho(\mathbf{r})=\rho_0+\psi(\mathbf{r})+\psi^*(\mathbf{r}) , \tag{1}$$

where the Fourier spectrum of ψ contains only those wave vectors $\mathbf{q}$ with $|\mathbf{q}|\approx q_0=2\pi/d$, where d is the smectic-layer spacing. Unlike the usual smectic order parameter of the noncovariant de Gennes model [i.e., $\tilde{\psi}\equiv\psi\exp(-iq_0z)$], ψ exhibits rapid spatial oscillations corresponding to the smectic layering.

The Chen-Lubensky free energy can be written as a sum of three terms,

$$F_{\mathrm{CL}}[\psi,\hat{\mathbf{n}}]=F_{\text{de Gennes}}[\psi,\hat{\mathbf{n}}]+F_D[\psi,\hat{\mathbf{n}}]+F_{\mathrm{Frank}}[\hat{\mathbf{n}}] . \tag{2}$$

The first term of Eq. (2) is a covariant version of the de Gennes model,

$$F_{\text{de Gennes}}=\int d^3\mathbf{r}(r|\psi|^2+\tfrac{1}{2}g|\psi|^4) + \int d^3\mathbf{r}[C_{\parallel}\hat{n}_i\hat{n}_j+C_{\perp}\delta^T_{ij}(\hat{\mathbf{n}})](\mathbf{D}_i\psi)(\mathbf{D}_j\psi^*) , \tag{3}$$

where $\mathbf{D}=\nabla-iq_0\hat{\mathbf{n}}$, $\delta^T_{ij}(\hat{\mathbf{n}})=\delta_{ij}-\hat{n}_i\hat{n}_j$, and $r_\psi=\alpha(T-T_{NA})$ with T_{NA} being the mean-field N–Sm-A transition temperature. One should note that, even if the smectic crystal is undistorted, ψ exhibits a rapid spatial oscillation corresponding to the density wave. Therefore, to obtain the usual de Gennes model one must replace ψ by $\tilde{\psi}\exp(iq_0z)$ and $\hat{\mathbf{n}}$ by $\hat{\mathbf{e}}_z+\delta\hat{\mathbf{n}}$, where $\hat{\mathbf{e}}_z$ is a unit vector in the z direction. The second term of Eq. (2), i.e., F_D, contains the fourth-order-gradient terms needed to describe the ring in x-ray-scattering intensity associated with N–Sm-C pretransitional fluctuations. It is given by

$$F_D=\int d^3\mathbf{r}[D_{\perp}\delta^T_{ij}\delta^T_{kl}(D_iD_j\psi)(D_kD_l\psi)^*] . \tag{4}$$

The last term of Eq. (2) is the Frank free energy describing the director elasticity

$$F_{\mathrm{Frank}}=\tfrac{1}{2}\int d^3\mathbf{r}\{K_1(\nabla\cdot\hat{\mathbf{n}})^2+K_2(\hat{\mathbf{n}}\cdot\nabla\times\hat{\mathbf{n}})^2 +K_3[\hat{\mathbf{n}}\times(\nabla\times\hat{\mathbf{n}})]^2\} , \tag{5}$$

where K_1, K_2, and K_3 are the splay, twist, and bend elastic constants.

In the absence of chirality, the equilibrium phase diagram is determined by minimizing F_{CL}. This gives the phase diagram in Fig. 3. Observe the presence of the Sm-A–Sm-C phase boundary at $C_\perp=0$. This can be understood by observing that gradient terms in F_2 tend to align the layer normal $\hat{\mathbf{q}}$ parallel to the director $\hat{\mathbf{n}}$. For $C_\perp<0$, θ defined by $\cos(\theta)\equiv\hat{\mathbf{q}}\cdot\hat{\mathbf{n}}$ is given by $\tan^2\theta=\tan^2\theta_0\equiv -C_\perp/(2D_\perp q_0^2)$. In the literature, one often finds the Sm-A–Sm-C transition described using the $\mathbf{c}$ director which is defined to be the component of $\mathbf{n}$ lying in the plane of the smectic layers, i.e.,

$$\mathbf{c}\equiv(I-\hat{\mathbf{N}}\hat{\mathbf{N}})\hat{\mathbf{n}} , \tag{6}$$

where $\hat{\mathbf{N}}$ is the layer normal and I is the unit matrix. In the absence of smectic-layer strain, the Sm-A–Sm-C transition can be described using free energy of the form $F_{A\text{-}C}=r_cc^2+g_cc^4$, where r_c changes sign at the Sm-A–Sm-C transition. In terms of de Gennes model parameters, one can show that $r_c=C_\perp|\psi_0|^2q_0^2$. $F_{A\text{-}C}$ exhibits an x-y symmetry which, of course, would be reduced by imposing strain. Simply stated, strain aligns the $\mathbf{c}$ director. This director alignment effect has important implications for the TGB_A-TGB_C transition to be discussed in Sec. V A.

In addition to the A-C boundary, there are two other second-order phase boundaries n this model. These are the N–Sm-A, and the N–Sm-C boundaries given by $r=r_{N\text{-}A}=0$ and $r=r_{N\text{-}C}=|C_\perp|^2/4D_\perp$, respectively. (See Fig. 3.) For a more detailed discussion of the nonchiral model the reader is referred to Ref. [16].

In the presence of chiral molecules, the phase diagram is determined not by minimizing F_{CL} but by minimizing the Gibbs density,

$$G=F-h\int d^3\mathbf{r}\,\hat{\mathbf{n}}\cdot\nabla\times\hat{\mathbf{n}} . \tag{7}$$

The "external field" h, conjugate to the twist $\hat{\mathbf{n}}\cdot\nabla\times\hat{\mathbf{n}}$, will be called the chirality. In the absence of layering, the cholesteric twist k_0, and pitch length P are related to the chirality by $k_0\equiv 2\pi/P=h/K_2$. However, as the temperature decreases, layering occurs and the twist tends to be

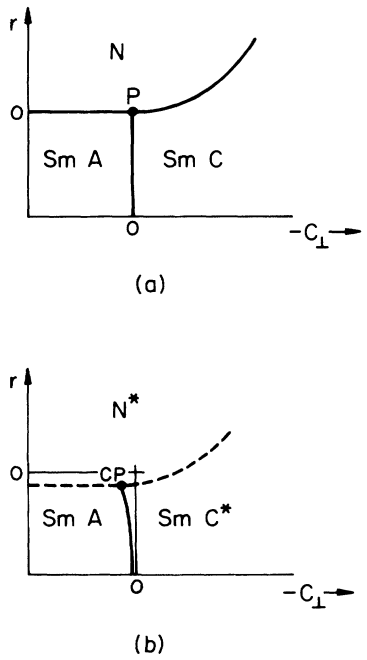

FIG. 3. Mean-field phase diagram for the CL model in the $(r,C_\perp)$ plane when $h=0$. The phase diagram displays the nematic (N), smectic-A (Sm-A), and smectic-C (Sm-C) phases. Also present is the N-A-C Lifshitz point P, where the N, Sm-A, and Sm-C phases meet. All the phase boundaries in this diagram are second order.

expelled. Indeed, in an undislocated Sm-A sample, twist can only penetrate a distance

$$\lambda_2=\left[\frac{K_2}{2C_\perp q_0^2\psi_0^2}\right]^{1/2}=\left[\frac{K_2 g}{2C_\perp q_0^2|r|}\right]^{1/2}. \tag{8}$$

As discussed in Ref. [4] the size of λ_2 relative to the smectic correlation length ξ determines the nature of twist expulsion. In particular, if the Ginzburg parameter

$$\kappa\equiv\frac{\lambda_2}{\xi}=\frac{1}{C_\perp q_0}\left[\frac{gK_2}{g}\right]^{1/2} \tag{9}$$

is less than $1/\sqrt{2}$, then the expulsion is complete in the sense that the system will either expel twist entirely or will phase separate into cholesteric and smectic regions. In this case the smectic is said to be type I. If, however, $\kappa>1/\sqrt{2}$ then the smectic is said to be type II. In this case, the TGB$_A$ phase will occur, separating the cholesteric and Sm-A phases on the (h,T) plane. This phase consists of a twisted stack of grain boundaries each consisting of a row of parallel equispaced screw dislocations. (See Fig. 1.) As mentioned in the caption, this phase is characterized by quasi-long-range Sm-A order in all directions perpendicular to the pitch axis, but short-range Sm-A correlations along the pitch axis.

Observe that the above twist penetration depth diverges as $C_\perp$ vanishes, i.e., as the Sm-A–Sm-C phase boundary is approached. Consequently, the smectic changes from type I to type II when $C_\perp=\sqrt{gK_2}/(2q_0)$ is approached. At this point, the first-order N^*–Sm-A phase boundary will bifurcate into a pair of second-order phase boundaries (the N^*–TGB$_A$ and TGB$_A$–Sm-A). These boundaries are called the upper critical temperature (T_{c2}) and lower critical temperature (T_{c1}) lines, respectively. (See the phase diagrams in Figs. 11–13.) Near the upper critical temperature, the smectic order parameter of the TGB$_A$ is

$$\psi(\mathbf{r})=\sum_i \psi_0\exp(i\mathbf{q}_\perp^i\cdot\mathbf{r}+iq_0u_i)\exp[-\tfrac{1}{2}(x-x_i)^2/\xi^2], \tag{10}$$

where $x_i=il_b$, $l_b\sim\xi\equiv 1/\sqrt{q_0k_0}=\sqrt{Pd}/(2\pi)$, and $\mathbf{q}_\perp^i\approx q_0\hat{\mathbf{n}}(x_i)$. Each term in this sum corresponds to a two-dimensional smectic slab of width ξ. The sum, of course, gives the twisted stack of slabs structure of the TGB$_A$. u_i is the displacement of the ith slab along the smectic-layer normal. This form of the TGB$_A$ was determined by a stability analysis [4] of the cholesteric, with respect to the development of smectic layering. That analysis was quite similar to Abrikosov's derivation of the spatial dependence of the Ginzburg-Landau order parameter of the triangular vortex lattice.

One of the most theoretically interesting features of the above form of the TGB$_A$ is that $l_b/P\sim\sqrt{d/P}/2\pi$ is experimentally adjustable. A detailed examination of the energetics reveals that there is a weak tendency for the TGB to lock in at any given rational values of l_b/P, thereby producing a commensurate TGB. In particular, if the TGB$_A$ is locked into a state with $l_b/P=p/q$, then the angle between adjacent slabs is $k_0l_b=2\pi p/q$. As will become clearer from our discussion of Sec. V A, the macroscopic properties of the commensurate TGB will often exhibit a q-fold screw symmetry. If $q\neq 4$ or 6, this symmetry is noncrystallographic and the commensurate TGB is a type of quasicrystal. We see then that u_i are phasons of the quasicrystal. Of course, not all of the u_i are independent phason degrees of freedom, since the energetics will determine all sums $\sum_i u_i$, for which $\sum_i \mathbf{q}_\perp^i=0$.

Next consider the x-ray-scattering intensity of the commensurate and incommensurate TGB. The x-ray scattering intensity of the incommensurate TGB is intense on the surface of a Bragg cylinder of radius q_0 and height $1/\xi$. See Fig. 4. The x-ray-scattering intensity of the commensurate TGB depends on whether q is even or odd. If q is odd, Bragg spots occur at $(Jk_0/p, Iq_\perp^{K/2})$, for any integers J and I, and where $q_\perp^{K/2}$ was defined following Eq. (10) and where $K=0,\ldots,2q-1$. As can be seen from the form of the TGB given in Eq. (10), only those spots with $I=1$ exist as $T\to T_{c2}$. For q even, spots exist at $(Jk_0/p, I\mathbf{q}_\perp^K)$ where $K=0,\ldots,q-1$, and where I is an arbitrary integer but J is even. Again, only the $I=1$ spots survive in the $T\to T_{c2}$ limit. The Bragg spots lie on

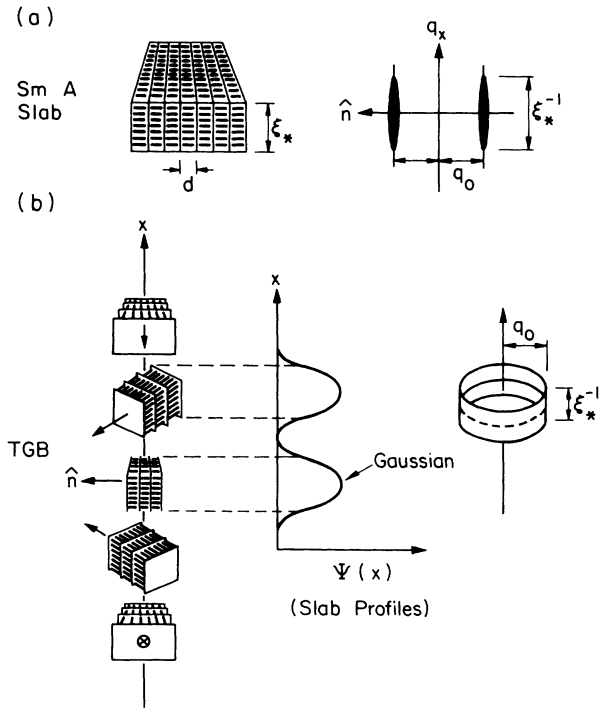

FIG. 4. (a) A Sm-A slab and the corresponding x-ray-scattering intensity. The latter is a pair of Bragg rods whose height is inversely proportional to the slab width. They are parallel to the slab normal and are displaced from the pitch axis by $\pm q_0\hat{\mathbf{N}}=(2\pi/d)\hat{\mathbf{N}}$, where d is the smectic-layer spacing and $\hat{\mathbf{N}}$ is the layer normal. (b) The incommensurate TGB$_A$ phase and the corresponding x-ray-scattering intensity. This is simply an in-plane powder average of the rods shown in (a). We have also plotted the order-parameter profile, i.e., $|\psi(x)|$, of the stack of slabs as a function of x, the pitch axis coordinate. The profile of a (Sm-A) slab is the (Gaussian) Landau-orbit solution of the linearized Ginzburg-Landau equations.

a vertically stacked q-fold symmetric axial [18] lattice [19]. The symmetry group of the lattice of Bragg spots (i.e., the Laue group G_L) is D_q. The group D_q is generated by a q-fold rotation $\mathcal{R}_q$ about the pitch axis and a π rotation d about a dihedral axis perpendicular to the pitch axis.

The detailed form of the phase diagram for $C_\perp > 0$ was determined in Ref. [5]. Here we shall merely summarize some of the main results. We found that the upper critical temperature is given by

$$r_{c2} = \begin{cases} -C_\perp q_0 h/K_2, & C_\perp \gg D_\perp q_0 k_0 \\ -A' D_\perp q_0^2 (h/K_2)^2, & C_\perp \ll D_\perp q_0 k_0 \end{cases} \tag{11}$$

where A' is a slowly varying function of $C_\parallel/(2D_\perp q_0^2)$ and $k_0 \simeq h/K_2$. We also found that the lower critical temperature is given by

$$r_{c1} = \begin{cases} -\dfrac{dg}{\pi C_\perp \ln\kappa^2} h, & C_\perp \gg (D_\perp |r|)^{1/2} \\ \left[-\dfrac{2dg}{D_\perp^{1/2}} \right]^{2/3}, & C_\perp \ll (D_\perp |r|)^{1/2} . \end{cases} \tag{12}$$

These results imply that the TGB_A phase occurs over a temperature interval $\Delta T = B T_{N\text{-}A} (k_0/q_0)^{2/3}$, where B is a constant of order unity. Using this, we estimated that, in nP1M7, the TGB_A phase could occur over a temperature interval of roughly 10–20 deg, which is consistent with the 7 °C temperature interval observed in nP1M7.

III. FORMATION OF Sm-C SLABS IN A CHOLESTERIC PHASE

Having reviewed the physics of the Sm-A side of the CL-model phase diagram, we now wish to analyze the CL model on the Sm-C^* side (i.e., $C_\perp < 0$) of the phase diagram. This analysis will determine the nature of the phase which develops when the cholesteric phase becomes unstable with respect to smectic layering.

We begin by observing that N^* develops smectic layers when some eigenvalue of the stability kernel

$$\frac{\delta^2 F}{\delta\psi^*(\mathbf{r})\delta\psi(\mathbf{r}')} = (\mathcal{C} + \mathcal{D} + r)\delta(\mathbf{r} - \mathbf{r}') , \tag{13}$$

where

$$\mathcal{C} \equiv -[C_\parallel \hat{n}_i \hat{n}_j + C_\perp \delta_{ij}^T(\hat{\mathbf{n}})]\mathbf{D}_i \mathbf{D}_j \tag{14}$$

and

$$\mathcal{D} \equiv D_\perp \mathbf{D}_l \mathbf{D}_k \delta_{kl}^T(\hat{\mathbf{n}}) \delta_{ij}^T(\hat{\mathbf{n}}) \mathbf{D}_i \mathbf{D}_j , \tag{15}$$

becomes negative at some temperature $T_{c2}(h)$.

In spite of this layering, the induced director distortion $\delta\hat{\mathbf{n}}$ is negligible near T_{c2} since $\delta\hat{\mathbf{n}} = O(\psi \mathbf{D} \psi)$. So near T_{c2},

$$\hat{\mathbf{n}}(\mathbf{r}) \approx \hat{\mathbf{n}}_0(x) \equiv [0, \cos(k_0' x), \sin(k_0' x)] ,$$

where $2\pi/k_0' \approx 2\pi/k_0 = P$. Since the only explicit spatial dependence of the stability kernel is through $\hat{\mathbf{n}}_0(x)$, the kernel is translationally invariant in the plane perpendicular to the pitch axis. This implies that the form of the least stable modes is

$$\psi(\mathbf{r}) = \phi_{q\perp}(x) \exp(i \mathbf{q}_\perp \cdot \mathbf{r}) , \tag{16}$$

where the vector $\mathbf{q}_\perp$ lies in the plane perpendicular to the pitch axis. Physically, we expect that $\phi_{q\perp}(x)$ will be large only for x such that $\tan^{-1}[\hat{\mathbf{n}}(x) \cdot \hat{\mathbf{q}}_\perp] \approx \pm\theta$, where θ is the equilibrium angle between the layer normal and the director in a bulk Sm-C sample. In fact, there are two vectors, $\mathbf{q}_\perp^\pm = q_\perp(0, \cos(k_0 \bar{x} \pm \theta), \sin(k_0 \bar{x} \pm \theta))$, which are simultaneously perpendicular to the pitch axis and are at an angle θ with respect to the director. (See Fig. 5.) Consequently, there are also two Bloch functions $\phi_{q_\perp^+}(x)$ and $\phi_{q_\perp^-}(x)$, which describe the two types of smectic slabs that may condense near $\bar{x}$.

Next we define $H(\nabla_\perp, \partial_x) \equiv [\mathcal{C} + \mathcal{D} + r]$ and observe that $\phi_{q_\perp}^\pm(x)$ are eigenfunctions of $H(q_\perp^\pm, \partial_x, x)$ which exhibits an explicit periodic (with period P) dependence on the pitch axis coordinate x. This implies, according to Bloch's theorem, that the spectrum of H consists of bands and the corresponding eigenfunctions are of the form $u(x)\exp(ikx)$, where $u(x) = u(x + P)$. However, one may verify that if $k_0 \ll q_0$, then the bandwidth is exponentially narrow. Therefore, we can consider the associated Wannier functions to be a nearly degenerate set of nearly exact least stable eigenmodes. Because these functions (unlike the Bloch functions) are spatially localized, one may then expand H in powers of $k_0(x - \bar{x})$. In the language of quantum mechanics, this is merely expanding about the potential well minima in an attempt to approximate H by a harmonic-oscillator Hamiltonian. For $C_\perp > 0$ this expansion indeed reduces H to the harmonic-oscillator form. However, if $C_\perp < 0$ the expansion yields

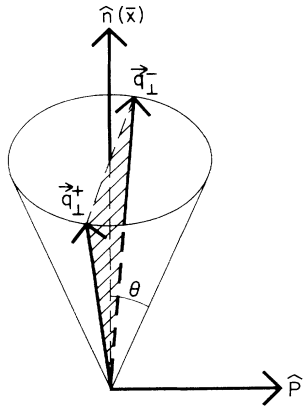

FIG. 5. The smectic-layering wave vector $\mathbf{q}_\perp = \mathbf{q}^+$ or $\mathbf{q}^-$. These directions are obtained as follows. First, we demand that less than $(\mathbf{q}, \hat{\mathbf{n}}(\bar{x}))$ equals θ, the angle between the smectic-layer normal and the director in a bulk sample of Sm-C. Second, we demand that $\mathbf{q}_\perp$ lies in the plane perpendicular to the pitch axis. The latter condition is required by the translation invariance of the linearized CL equations in the plane perpendicular to $\hat{\mathbf{P}}$. These two choices for $\mathbf{q}_\perp$ give two types of Sm-C slabs (+ or −) which are related by a π rotation about an axis perpendicular to the pitch axis. The latter is a symmetry of the TGB_A point group (D_q) which is spontaneously broken by the Ising-like TGB_A-TGB_C transition.

$$H \approx \left[r - \frac{C_\perp^2}{4D_\perp} \right] + \tfrac{1}{2}\omega_c^2 [x^2 + \mu(xp^2 + p^2 x)] + \beta(x^2 p^2 + p^2 x^2) + D_\perp p^4 , \tag{17}$$

where $p \equiv -i\partial_x$ and the coefficients are

$$\tfrac{1}{2}\omega_c^2 = -2C_\perp (q_0 k_0)^2 \left[1 + \frac{C_\parallel}{4D_\perp q_0^2} \right] , \tag{18}$$

$$\mu = -\left[\frac{D_\perp}{2|C_\perp| k_0^2 q_0^2} \right]^{1/2} \left[1 + \frac{C_\parallel}{4D_\perp q_0^2} \right]^{-1} , \qquad \beta = -D_\perp (q_0 k_0)^2 \left[1 + \frac{C_\perp}{2D_\perp q_0^2} \right] . \tag{19}$$

Several observations about this expansion of H are in order: The first is that no p^2 term occurs in H. This could have been anticipated by considering a derivation of those terms which remain in the limit of infinite pitch, i.e., $\hat{\mathbf{n}}_0(x) = (0,1,0)$. In that limit, we may take $\phi_{q\perp} = \exp(ipx)$, which corresponds to tipping the layer normal along the x axis. The energy cost of this tipping is

$$\begin{aligned} F_{\rm CL}(q_\perp, p) &= |\psi|^2 \{ D_\perp [(q_{\perp\perp} + p\hat{\mathbf{x}})^2 - q_0^2 \tan^2\theta]^2 + C_\parallel (q_{\perp\parallel} - q_0)^2 \} \\ &= D_\perp |\psi|^2 p^4 + \text{const} , \end{aligned} \tag{20}$$

where $q_\perp = (0, q_{\perp\parallel}, q_{\perp\perp})$. Now $F_{\rm CL} \sim r_c c^2 \sim p^4$ because $\delta|c| \sim p^2$ for Sm-C-layer tipping. This should be compared to the result obtained for $C_\perp > 0$,

$$F_{\rm CL} = C_\perp |\psi|^2 p^2 + D_\perp |\psi|^2 p^4 . \tag{21}$$

This is proportional to p^2 because Sm-A-layer tipping gives $\delta|c| \sim p$.

The second observation is that the eigenstates of H are localized at $x = 0$. This would imply a two-dimensional slab of Sm-C where the angle between the director and the layer normal $q_\perp$ is θ_0, the bulk Sm-C director angle. As discussed below, the μ term causes the Sm-C director angle to weakly deviate from this bulk value by $O((k_0/q_0)^{2/3})$.

To proceed further we introduce the cannonical variables $q = x + \mu p^2$ and $p' = p$. Then $H = H_0 + H_1 + H_2 + H_3$ where

$$H_0 = \tfrac{1}{2}\omega_c^2 q^2 + D'_\perp p^4 , \tag{22}$$

$$H_1 = \beta(q^2 p^2 + p^2 q^2) , \tag{23}$$

$$H_2 = -\beta\mu(qp^4 + 2p^2 qp^2 + p^4 q) , \tag{24}$$

$$H_3 = 2\beta\mu^2 p^6 , \tag{25}$$

and $D'_\perp = D_\perp - \tfrac{1}{2}\mu^2\omega_c^2$. One may readily show that the spectrum of H_0 is $E_0\kappa_n$; $n = 1, \ldots$ where

$$E_0 = (4D_\perp q_0^4) \left[\frac{k_0}{q_0} \right]^{4/3} R \left[\frac{C_\perp}{4D_\perp q_0^2}, \frac{C_\parallel}{4D_\perp q_0^2} \right] , \tag{26}$$

$R(x_\perp, x_\parallel) = [(1 + x_\parallel) x_\parallel x_\perp^2]^{1/3}$, and κ_n $(n = 1,2,\ldots)$ are positive numerical constants. The scaling arguments which give the spectrum of H_0 may also be used to show that $H_{1,2,3}$ perturb the H_0 spectra by $O(E_0(k_0/q_0)^{2/3})$. Their contribution to H may be neglected since $P \gg d$. Hence the eigenvalues of the stability kernel in Eq. (13) are $\varepsilon_n = E_0[\kappa_n + O((k_0/q_0)^{2/3})]$. The layering instability occurs when ε_0 changes sign which occurs at $T = T_{c2} \equiv T_{N\text{-}A} + r_{c2}/\alpha$.

Comparing this result with that of Eq. (11) might suggest that the two T_{c2} curves at $C_\perp = 0$ are mismatched by $\Delta r \sim D_\perp (q_0 k_0)^2$. This is an artifact: When $|C_\perp| < D_\perp q_0 k_0$, the perturbation H_1 is no longer negligible and the above analysis breaks down. In fact, the required continuity of the spectral flow of H implies that r_{c2} saturates when $-C_\perp < D_\perp q_0 k_0$. Therefore, we conclude that

$$r_{c2} = \begin{cases} \dfrac{C_\perp^2}{4D_\perp} - \kappa_0 (4D_\perp q_0^4) \left[\dfrac{h}{q_0 K_2} \right]^{4/3} R \left[\dfrac{C_\perp}{4D_\perp q_0^2}, \dfrac{C_\parallel}{4D_\perp q_0^2} \right], & C_\perp \gg D_\perp q_0 k_0 \\ -A' D_\perp q_0^2 k_0^2, & C_\perp \ll D_\perp q_0 k_0 . \end{cases} \tag{27}$$

Next we consider the eigenfunctions of H_0. These have a finite width along the pitch axis which is given by

$$\xi_* = \begin{cases} \dfrac{d}{2\pi} \left[\dfrac{q_0}{k_0} \right]^{1/3} \left[\dfrac{D_\perp q_0^2}{|C_\perp|} \right]^{1/6}, & |C_\perp| \gg D_\perp q_0 k_0 \\ 1/\sqrt{q_0 k_0}, & |C_\perp| \ll D_\perp q_0 k_0 . \end{cases} \tag{28}$$

The approximate eigenstates given in Eq. (16) are two-dimensional slabs of Sm-C. Unlike the Sm-A slabs which occur in the TGB$_A$, the order parameter is not Gaussian. We now observe that $\phi(q)$, being centered at $q = 0$, implies that $\phi(x)$, the corresponding eigenfunction of H prior to canonical transformation, will be centered at $x = \mu\langle p^2 \rangle$. This, in turn, implies that $\theta = \theta_0 + k_0 \mu \langle p^2 \rangle$. Using the scaling properties of the eigenfunctions, one finds that

$$\theta - \theta_0 = -\text{const} \times \left[\frac{C_\perp}{2D_\perp q_0^2} \right]^{-1/3} \left[\frac{k_0}{q_0} \right]^{2/3} , \qquad C_\perp \gg D_\perp q_0 k_0 \tag{29}$$

where the constant depends on the ratio $C_\parallel / 4D_\perp q_0^2$. Therefore, if $P \gg d$, the director angle of a slab will nearly equal that of bulk Sm-C.

At the layering instability, slabs of this form nucleate throughout the cholesteric sample until a one-

dimensional lattice of slabs forms. This is the TGB_C phase. The smectic order parameter for the TGB_C is

$$\psi(\mathbf{r})=\sum_s \phi(x-x_s)\exp[i\mathbf{q}_s^{\pm}\cdot\mathbf{r}+iq_0u_s/\cos\theta]\ , \tag{30}$$

where u_s is an arbitrary phason angle of the slab, $x_s=sl_b$, and where $l_b\sim\xi_*$. As with the TGB_A, the destructive interference of the smectic order in adjacent slabs gives rise to a row of screw dislocation lines with spacing $l_d\simeq d/(k_0l_b)$. The large (i.e., extensive) number phason angles in Eq. (30) are hydrodynamic Goldstone modes [20] of both the TGB_C as well as the TGB_A phases.

To prove (within mean-field theory) that the TGB_C exists, one must demonstrate that this layering instability (i.e., the N^*-TGB_C transition) is not preempted by the direct N^*–Sm-C^* transition. The latter occurs at $r_{N^*C^*}$ given by

$$r_{N^*C^*}=-\left[\frac{g}{K_2}\right]^{1/2}h+\frac{1}{4D_\perp q_0^4}\left[-C_\perp q_0^2+\frac{1}{2}\left[\frac{K_2g}{K_3^2}\right]^{1/2}(3)h\right]^2 . \tag{31}$$

Using Eqs. (27) and (31) we find that for small h, $r_{N^*C^*}<r_{c2}$ provided

$$-C_\perp<(4D_\perp q_0^2)\frac{K_3}{K_2}\ . \tag{32}$$

This is the $C_\perp<0$ analog of the Ginzburg criterion which states that the flux lattice can occur in a superconductor only when $\kappa>1/\sqrt{2}$. The T_{c2}, T_c, and the T_{c1} (see Sec. IV) lines will meet when $C_\perp$ satisfies the equality in Eq. (32).

IV. DISLOCATIONS AND GRAIN BOUNDARIES AND THE Sm-C^*–TGB_{C^*} TRANSITION

In the preceding section we found that the N^* became unstable with respect to the formation of the TGB_C phase as T dropped below $T_{c2}(C_\perp)$. Our next task is to consider Sm-C^* dislocations and grain boundaries with an eye towards understanding possible TGB phases which might be constructed from Sm-C^*.

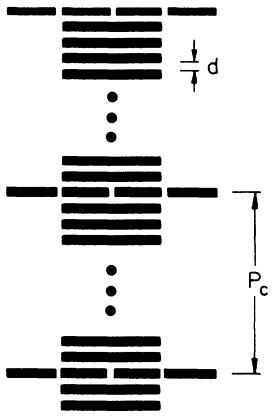

FIG. 6. The Sm-C^* phase viewed as an incommensurate smectic. Two sets of layers occur in the Sm-C^* phase. The first are the smectic density-wave layers with spacing d. The second consist of the constant orientation planes of the **c** director. These are called helilayers. Their spacing P_c is the periodicity of the Sm-C^* helicoidal modulation. A strained Sm-C^* sample can be described by the displacements u_1 and u_2, of, respectively, the density-wave layers and the helilayers, along the z axis. (See Sec. IV.)

Before beginning our discussion, it is useful to recall [21,22] a few facts about Sm-C^*. The undistorted Sm-C^* is identical to the undistorted Sm-C expect that the **c** director twists around as one moves along the layer normal direction ($\hat{\mathbf{z}}$). More generally, a strained Sm-C^* crystal would be described by

$$\mathbf{c}=c(\sin\{q_c[z+u_2(r)]\},\cos\{q_c[z+u_2(r)]\},0)\ ,$$

where $u_2(\mathbf{r})$ is the displacement of the constant **c** planes ("heli layers"). It is useful to view the Sm-C^* phase as a type of incommensurate smectic [23] where the spacing $P_c=2\pi/q_c$ of the helilayers is incommensurate with the density-wave layer spacing d. See Fig. 6. Of course, unlike the usual incommensurate smectic, the ratio of the two layer spacings d/P_c is $\sim10^2$ rather than ~2. Nevertheless, the two systems are formally very similar. In particular, both exhibit similar long-wavelength physics described by

$$F_{ic}(u_1,u_2)=\int d^3\mathbf{r}(\tfrac{1}{2}\{B_1(\partial_zu_1)^2+K_{11}(\nabla_\perp^2u_1)^2+B_2(\partial_zu_2)^2+K_{22}(\nabla_\perp^2u_2)^2+D[\nabla_\perp(u_1-u_2)]^2\}$$
$$+B_{12}(\partial_zu_1)(\partial_zu_2)+K_{12}(\nabla_\perp^2u_1)(\nabla_\perp^2u_2))\ , \tag{33}$$

where $u_1(\mathbf{r})$ is the displacement of the density-wave layers. The elastic constants in $F_{\rm inc}$ may be calculated in terms of the de Gennes model parameters. However, we wish to merely note that B_1 and B_2 are proportional to $|\psi|^2$ and $|\mathbf{c}(q_c)|^2$, respectively, and that D is proportional to $|\psi|^2|\mathbf{c}(q_c)|^2$. Following Lubensky, Ramaswamy, and Toner's [23] discussion of incommensurate smectics, it is useful to introduce the phason and phonon variables: $u\equiv(1-s)u_1+su_2$ and $w\equiv u_2-u_1$. Of course, the Sm-C^* phason should not be confused with the TGB_A phasons discussed in Sec. II. If we choose $s=(B_2+B_{12})/(B_1+B_2+2B_{12})$, then the phason and phonon variables decouple in the long-wavelength limit. One thereby obtains $F_{\rm inc}=F_{\rm sm}(u)+F_{XY}(w)$, where $F_{\rm sm}=\frac{1}{2}B_u(\partial u)^2+\frac{1}{2}K_u(\nabla_\perp^2u)^2$ is the usual Landau-Peirles smectic free energy and $F_{xy}(w)=\frac{1}{2}D|\nabla_\perp w|^2+\frac{1}{2}B_w(\partial_zw)^2$ is an anisotropic XY model. The elastic constants of the decoupled free energy are $B_u=(B_1+B_2=B_{12})$, $B_w=[s^2B_1+(1-s)^2B_2-2s(1-s)B_{12}]$, and $K_u=K_{11}+K_{22}=K_{12}$. In the above expression for $F_{\rm inc}$,one notices

that a rotation, of one set of layers relative to the other (i.e., $\nabla w = \text{const}$), would cost a finite energy. Of course, a rotation of both sets of layers, $\nabla u = \text{const}$, costs nothing.

In addition to having similar elasticity theories, the Sm-C^* and the incommensurate smectic phases have similar defect structures. In particular, as one circumnavigates any line defect, u_1 and u_2 must change by an integral multiple of d and P_c, respectively. This means that

$$\oint dl \cdot \nabla u_i = b_i = m_i l_i \ ,$$

where $l_1 = d$ and $l_2 = P_c$. The vector (b_1, b_2) is the Burgers vector of the smectic. The set of allowed Burgers vectors lies on the lattice shown in Fig. 7. Any given Burgers vector can correspond to either a screw or edge dislocation depending on whether the dislocation line is parallel or perpendicular to the z axis, respectively. The screw dislocation, with Burgers vector $(d,0)$, is known as a wedge-screw dispiration [24,25]. It has a nematic core with a radius ξ and converts to an ordinary Sm-A screw dislocation at the Sm-A–Sm-C^* transition. Dislocations with a Burgers vector $(0,P_c)$ have Sm-A-like cores with a much larger core radius r_c. These dislocations will, hereafter, be called "heliscrew dispirations." They disappear at the Sm-A–Sm-C^* transition, and have no analogs in the Sm-A phase.

It is worthwhile to mention how one constructs the wedge-screw dispiration using a Volterra construction. Usually a screw dislocation is constructed by shifting the smectic on one side of the Volterra cut by a distance d relative to the other side of the cut surface. However, Kleman [24] has pointed out that the c angle would jump by $q_c d$ across the cut surface. Therefore, to obtain a line defect which is continuous across the cut, one must also rotate the director on one side of the cut as well. We see that this defect is simultaneously a wedge disclination as well as a screw dislocation. Thus follows the name "wedge screw."

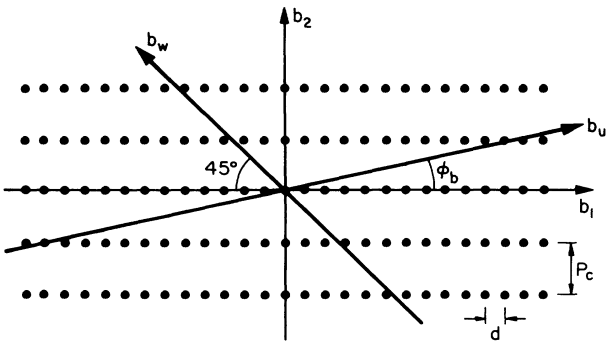

FIG. 7. The Burgers lattice of the Sm-C^* phase. $b_1 = \oint dl \cdot \nabla u_1$ and $b_2 = \oint dl \cdot \nabla u_2$ are components of the Burgers vector of the screw or edge dislocation. The topologically allowed dislocations have $(b_1, b_2) = (nd, mP_c)$ and may be represented as points on a Burgers lattice. The phonon and phason components b_u and b_w of a dislocation are the projections of the Burgers lattice point onto the b_u and b_w axes shown in the figure. Since $\tan\phi_b$ is, in general, irrational, no dislocation has $b_w = 0$. As a result, all screw dislocations have logarithmically divergent energies.

To discuss the energetics of these dislocations, it is useful to define the u and w components of the Burgers vectors: $b_u \equiv (1-s)b_1 + sb_2$ and $b_w \equiv (b_2 - b_1)$. Using $F_{\text{inc}}(u,w)$, Lubensky, Ramaswamy, and Toner [23] have calculated the energy of the dislocations occurring in incommensurate smectics. Their results give the wedge-screw and heliscrew energies: $\varepsilon_{\text{WS}} = \varepsilon_{\text{core}}^{\text{WS}} + Dd^2 \ln(l/\xi)$ and $\varepsilon_{\text{HS}} = \varepsilon_{\text{core}}^{\text{HS}} + DP_c^2 \ln(l/r_{\text{HS}})$, where l is the sample size. Remarkably, the second set of layers causes the dislocation energies to diverge logarithmically. The wedge-screw core energy is

$$\varepsilon_{\text{core}}^{\text{WS}} = \frac{Kd^2}{2\pi\lambda_{2\perp}^2} \ln\kappa [1 + O(c^2)] \ . \tag{34}$$

This is the contribution to the wedge-screw energy from the dislocation core, i.e., the sample volume contained in a cylinder of radius $\sim\lambda_2$ centered about the dislocation core [26]. The heliscrew core energy $\varepsilon_{\text{core}}^{\text{HS}} \sim f_{A\text{-}C^*} r_{\text{HS}}^2$, where $f_{A\text{-}C^*}$ is the Sm-A–Sm-C^* condensation energy. The core size r_{HS} of the heliscrew is not the same as the core size of the wedge screw. r_{HS} may be estimated by minimizing the sum of phason and core energies with respect to r_{HS}. This gives $r_{\text{HS}} = DP_c^2/(2f_{A\text{-}C^*})$ which is proportional to c^2 within mean-field theory. With this choice of r_{HS}, the energy of a heliscrew becomes $\varepsilon_{\text{HS}} = DP_c^2 \ln(c_0 l/r_{\text{HS}})$, where c_0 is some constant of order unity. One may also calculate the energy of compound dislocations, and use this to identify their relative stability. Unfortunately, this task is complicated by the logarithmic dependence of the dislocation energy on sample size. One can, however, show that dislocations with $(b_1, b_2) = (nd, 0)$ will fragment into n wedge screws. One can also show, for an infinitely large sample, that dislocations of the form $(b_1, b_2) = (-nd, P_c)$ with n large will tend to fragment into m wedge screws and a compound dislocation, $(-n'd, P_c)$, where $n' = n - m$ is the integer closest to P_c/d.

Next we consider the construction of an isolated twist grain boundary. A grain boundary in Sm-C^* consists of interpenetrating rows of wedge screws and heliscrews. The spacings between the wedge screws and between the heliscrews must be chosen such that the grain boundary rotates both sets of layers by the same angle $\Delta\theta$. Otherwise, the smectic layers and helilayers will not be parallel far from the grain boundary plane which would cause the areal energy density of a grain boundary to diverge [27]. In particular, if the spacing of wedge screws and heliscrews is uniform (wedge-screw and heliscrew spacing equal to l_d and l_d^H, respectively) then $\Delta\theta = 2\tan^{-1}(d/2l_d) = 2\tan^{-1}(P_c/2l_d^H)$. To calculate the energy of an isolated grain boundary, one observes that $F_{\text{Sm}}(u)$ vanishes and, hence, only the phason strain energy contributes. The calculation of the phason strain energy is an electrostatic calculation in which dislocations act like charged lines with linear charge density b_w. To further simplify the calculation, we take advantage of the smallness of l_d/l_d^H and replace the row of wedge-screw lines with a sheet of uniform charge. One thereby finds that the phason configuration of a grain boundary lying in the xz plane with dislocations parallel to the z axis is

$$w=-\frac{P_c}{4\pi}\sum_n \frac{1}{|n|}\exp\left[\frac{2\pi n}{l_d}[ix-(\mathrm{sgn}n)|y|]\right], \quad (35)$$

where n is summed from $-N_{\max}$ to $+N_{\max}$ (excluding $n=0$), where $N_{\max}\sim l_d/r_{\mathrm{HS}}$ is an ultraviolet cutoff associated with the finite core radius of a heliscrew. Using Eqs. (34) and (35), we obtain the areal energy density of a Sm-C^* grain boundary

$$\frac{E^{\mathrm{GB}}_{\text{Sm-}C^*}}{A}=\left[\frac{\varepsilon^{\mathrm{core}}_{\mathrm{WS}}}{d}+\frac{DP_c}{2\pi}\ln\left[\frac{a_0P_c}{r_{\mathrm{HS}}\Delta\theta}\right]\right]\Delta\theta, \quad (36)$$

where A is the grain-boundary surface energy and $\Delta\theta$ is the grain-boundary rotation angle (i.e., the smectic on one side is rotated by an angle $\Delta\theta$ relative to that on the other side.) In the above expression, the term proportional to D includes both the dislocation interaction energy (mediated by the phason) and the heliscrew core energy. Unlike the energy of an isolated dislocation, the grain-boundary energy is finite. The Sm-C^* grain boundary energy should be compared with that of the Sm-A grain boundary

$$\frac{E^{\mathrm{GB}}_{\text{Sm-}A}}{A}=\frac{\varepsilon^{\mathrm{core}}_{\mathrm{screw}}\Delta\theta}{d}=\frac{K_2 d\Delta\theta}{2\pi\lambda_2^2}\ln\kappa. \quad (37)$$

We see that the Sm-C^* grain-boundary energy reduces to $E^{\mathrm{GB}}_{\text{Sm-}A}$ at the Sm-A–Sm-C^* transition (as expected). We also see that the Sm-C^* grain boundary energy has logarithmic corrections to the linear $\Delta\theta$ dependence. The $\Delta\theta\ln(\Delta\theta)$ dependence is a signature of the long-range phason interactions.

One can now imagine forming a new TGB phase (TGB_{C^*}), consisting of a twisted stack of the Sm-C^* grain boundaries with spacing $l_b=l_b^H=\theta/k_0$. There are, however, other possible structures for a TGB_{C^*}. To describe them, it is useful to define smectic boundaries and heliboundaries as grain boundaries consisting of only wedge-screw or heliscrew dislocations, respectively. Hence, the finite energy Sm-C^* grain boundary is a heliboundary superimposed on a smectic grain boundary. With these definitions, we can now introduce an alternative TGB_{C^*} structure. The alternative structure is a twisted stack of heliboundaries (with spacing l_b^H) superimposed on a twisted stack of smectic boundaries (with spacing $l_b\neq l_b^H$). (See Fig. 8.) This alternative structure will have a finite energy density provided that the average twist produced by the heliscrews, $k_0^H\approx P_c/(l_d^H l_b^H)$, equals that produced by the wedge screws, i.e., $k_0=d/(l_b l_d)$. In Sec. V B we will find a transition where the TGB_A becomes unstable to a TGB_{C^*} phase with this second structure. In addition, we will find that near the TGB_A–TGB_{C^*} transition $l_b^H\sim l_d^H$ but $l_b^H\gg l_b$.

Let us now briefly consider a possible Sm-C^*–TGB_{C^*} transition. Because of the logarithmic dependence of the phason strain energy on the heliscrew spacing [see, for example, Eq. (34)], the Sm-C^*–TGB_{C^*} transition is first order. The Sm-C^*–TGB_{C^*} transition, like the TGB_A–Sm-A, occurs when the chirality increases to some value h_{c1} where the Gibbs energy of the Sm-C^* decreases with the addition of dislocations. One can derive a formula for h_{c1} in terms of dislocation line energies, interaction energies, and dislocation twist. However, the resulting expression is not terribly useful, since the dislocation twist and interaction energies are difficult to evaluate. Nevertheless, one can argue that the TGB_{C^*}–Sm-C^* line joins continuously with the TGB_A–Sm-A line.

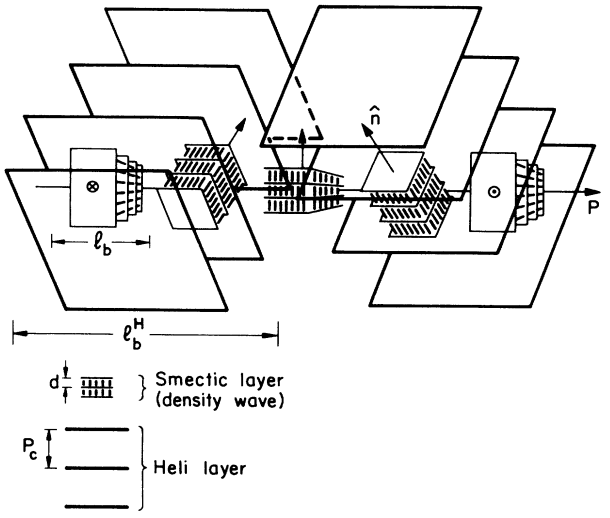

FIG. 8. The TGB_{C^*} phase. This structure consists of a twisted stack of helislabs superimposed on a twisted stack of smectic slabs. The layers in the smectic slabs are density waves, whereas the layers in the helislabs are helilayers. As is evident from the figure, the grain-boundary spacing of the smectic slabs l_b is much shorter than that of the helislabs l_b^H. One could also imagine a TGB_{C^*} structure with $l_b=l_b^H$. This would be the case if the TGB_{C^*} were composed of the finite energy Sm-C^* grain boundaries. (See Sec. IV.) However, the theory discussed in Sec. V B shows that, at the TGB_A–TGB_{C^*} transition, the TGB_{C^*} structure with $l_b/l_b^H\sim\sqrt{d/P_c}$ occurs.

It is useful to define the h_{c1} line as the union of all smectic to TGB phase boundaries. On the Sm-C^* side of the phase diagram, the h_{c1} line would, therefore, represent all instabilities of the Sm-C^* phase with respect to the formation of wedge screws and heliscrews. In particular, segments of the h_{c1} line on the Sm-C^* side of the phase diagram could represent Sm-C^*–TGB_{C^*}, Sm-C^*–TGB_C, or even Sm-C^*–TGB_A transitions. These h_{c1} line segments will connect the intersection of the TGB_A–Sm-A and Sm-A–Sm-C^* phase boundaries with the interaction of the N^*-TGB_c and the N^*—Sm-C^* phase boundary. (See Figs. 11–13.) In the discussion of Sec. V C, we will develop a clearer picture regarding which TGB phases are likely to be formed from the Sm-C^*.

V. THE TGB_A-TGB_C AND TGB_A-TGB_{C^*} TRANSITIONS

Even though the outlines of the phase diagram of the chiral Chen-Lubensky model are beginning to emerge,

there is still much to be done. In particular, we have not yet considered the TGB_A-TGB_C transition. At this transition, it is clear that the director field of the TGB_A is rotated, relative to the layer normals, about the pitch axis. Yet there remains some fundamental questions. In particular, it is not yet clear what (if any) symmetry is broken at this transition. Nor is it clear when the TGB_A-TGB_{C*} is replaced by a TGB_A-TGB_{C*} transition. There is, after all, a tendency for the chirality to produce Sm-C^*-like rather than Sm-C-like slabs.

The discussion in Secs. V A–V C is designed to answer these questions. In Sec. V A we will determine the TGB_A-TGB_C order parameter and discuss the various symmetries which may be broken at the transition. In Sec. V B we will derive a coarse-grained TGB_A stability operator from the Chen-Lubensky model. Then in Sec. V C we will analyze this coarse-grained stability operator. This analysis will determine (1) the conditions required for the TGB_{C*} phase to occur, (2) the location of the TGB_A-TGB_C and the TGB_A-TGB_{C*} phase boundaries, and (3) the structure of the multicritical points near the intersection of the h_{c1} and Sm-A–Sm-C^* lines.

A. Symmetry breaking at the TGB_A-TGB_C transition

At first glance, the symmetries of the TGB phases are confusing: Spatially averaged observables of the TGB phase, such as free energies, x-ray-scattering intensities, and correlation functions, can exhibit noncrystallographic q-fold screw axis, even when local properties, such as $\psi(\mathbf{r})$ do not. One must, therefore, distinguish between the symmetries of spatially averaged observables (known as macroscopic symmetries) and the symmetries of local observables. This distinction between macroscopic and local symmetries is now understood to be a general property of quasicrystals, incommensurate crystals [19], and even ordinary crystals with screw or glide axes [28]. In discussing such systems, the point group H_X of a phase X, refers to all *macroscopic* point-group symmetries of the phase. In particular, the point-group operation may leave the system invariant only to within translations, phason shifts, and so forth.

With this definition, we can now consider the point group of the cholesteric and the TGB_A. The cholesteric, of course, has a continuous screw symmetry. However, it is also invariant under d, a π rotation about an arbitrary dihedral axis perpendicular to the pitch axis. The dihedral symmetry d may be verified by examining the effect of d_y, a π rotation on $n_0(\mathbf{r})\equiv(0,\cos(k_0x),\sin(k_0x))$ about the $\hat{\mathbf{y}}$ axis. Moreover, a π rotation about any other axis, perpendicular to the pitch axis, would also leave $\hat{\mathbf{n}}$ invariant *to within a translation.* The point group of the cholesteric is, therefore, D_∞.

Next consider the point group of the incommensurate TGB_A, as described near h_{c2} by Eq. (10). In particular, consider the effect of a rotation $\mathcal{R}$ by an angle $2\pi\alpha$ about the pitch axis, followed by a translation by l_b along this axis. Together, these transformations have the same effect as the replacement $u_i\rightarrow u_{i-1}$. One can also show (for $\bar{x}_0=0$) that d_y has the same effect as $u_i\rightarrow u_{-i}$. Now since the macroscopic properties of the incommensurate TGB_A are independent of the $u_i's$, $\mathcal{R}$ and d are macroscopic symmetries. Moreover, a given rotation about the pitch axis can, to arbitrary precision, be written as $\mathcal{R}^n$ for some n. Therefore we conclude that the point-group symmetry of the incommensurate TGB_A, like that of the cholesteric, is D_∞. Of course, this does not imply that the N^* to incommensurate TGB_A transition is necessarily first order: The N^*-TGB_A transition spontaneously breaks the translation symmetry of the cholesteric.

Finally, we consider the commensurate TGB_A with $\alpha=2\pi p/q$. The effects of $\mathcal{R}$ and d are as described above. However, the macroscopic properties of the TGB_A depend on phason sums of the form $\sum_{i\in S}u_i$, where S is any set of slabs such that $\sum_{i\in S}q_\perp^i=0$. If q is prime, the only such sums are $T\equiv\sum_{i=1}^{q}u_i$ and $D_i\equiv u_{i+q}-u_i$, where $i=-\infty,\ldots,+\infty$. In general, the values of these sums depend on the detailed energetics and are difficult to calculate [15]. However, if the D_i are all equal, then the TGB_A point group is D_q, since T is an invariant. If q is not prime, then additional phason sums become observable. For example, if $\alpha=2\pi/9$, then the sums $A\equiv u_1+u_4+u_7$, $B\equiv u_2+u_5+u_8$, and $C\equiv u_3+u_6+u_9$ are all observable. In this case, if A, B, and C are all distinct but the D_i's are all equal, then the point-group symmetry is not D_9 but is, instead, C_3. In the remainder of this section, we will restrict our attention to TGB_A phases with D_q symmetry.

We can now explain the following paper of "coincidences" which occurred in the discussion in Sec. III. The first was that the cholesteric became simultaneously

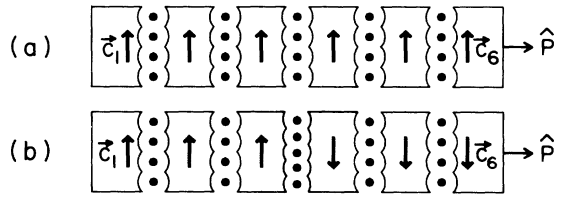

FIG. 9. (a) and (b) are schematic drawings of two TGB_C stacks. These are composed of a sequence of Sm-C slabs separated by grain boundaries. Dislocations within a grain boundary are denoted by a vertical row of dots. Although the slab orientation twists around as one moves along the pitch axis, we have for simplicity drawn the figure as if the dislocation lines and smectic-layer normals were oriented along the page normal. The arrow within each slab denotes the c director which prefers to point either up or down. This refers to the tendency of the twisting nematic director to, respectively, lag ahead or behind the layer normals by $\theta\approx\tan^{-1}(C_\perp/2D_\perp q_0^2)$. (a) consists of a ferromagnetic stack of up slabs, whereas in (B) there is an Ising domain wall separating up from down slabs. The domain wall is a high-angle grain boundary which is likely to be a common defect of the TGB_C.

unstable with respect to both slab types. The second coincidence was that the slab-profile function for the two slab types are equal. We now see why: The dihedral symmetry takes a plus slab centered at $x=\bar{x}$ with phase u into a minus slab centered at $\bar{x}'=-\bar{x}$ with phase $u'=u$. This explains why the two types of slabs are degenerate eigenmodes.

Now suppose the TGB_C consists of a *ferromagnetic* stack, i.e., a stack of all plus or all minus slabs. [See Fig. 9(a).] In this case, we see that the macroscopic dihedral symmetry of the TGB_A phase is broken at the TGB_A-TGB_C transition. If we define $\hat{N}(\mathbf{r})$ to be the local layer normal and $\mathbf{c}$ to be the c director defined in Eq. (7), then the TGB_A-TGB_C transition (like the Sm-A–Sm-C transition) may be described using $\langle \hat{\mathbf{N}}\times\mathbf{c}\rangle$ as the order parameter. The two transitions differ simply because the TGB twists act as a nonordering Ising anisotropy on the (xy-like) Sm-A–Sm-C^* transition.

Based on the above discussion, we expect that Ising-like domain walls can occur in the TGB_C. These domain walls, of course, divide the stack into sequences of slabs of the same type (either + or −). Therefore, one might ask whether the TGB_C ground state consists of a stack of like slabs (i.e., the ferromagnetic stack which was assumed above) or whether it consists of an alternating sequence of plus and minus slabs (i.e., an antiferromagnetic stack). (See Fig. 9.) This can be determined by the sign of the domain-wall energy. Consider, therefore, the interaction of two overlapping Sm-C slabs. A pair of like slabs will give a smaller interaction energy than a pair of opposite slabs, since the overlap of opposite slabs produces a higher density of repulsive screw dislocations. Hence, the TGB_C ground state is a twisted ferromagnetic stack.

Since only macroscopic symmetries are broken at the TGB_A-TGB_C transition, one may feel uncertain whether the Landau criterion can be applied to infer the possibility of a second order TGB_A-TGB_C transition. As discussed in Appendix A, the group theory does, in fact, allow a continuous TGB_A-TGB_C transition in spite of the absence of local symmetries. The discussion in the appendix also shows that several distinct TGB_A-TGB_C transitions are possible. These transitions are distinguished by the point-group symmetry of the TGB_C phase. In particular, one may have transitions in which the D_q symmetries TGB_A phase is transformed into $C_{q'}$ symmetric TGB_C, where $q=nq'$ for some $n\geq 1$.

B. Derivation of a coarse-grained stability theory

In the next two subsections, we will generalize the Chen-Lubensky analysis of the Sm-A–Sm-C transition to describe the TGB_A-TGB_C and TGB_A-TGB_{C^*} transitions. The purpose of this section is to construct a coarse-grained stability operator $\chi^{-1}(\nabla,r)$ describing instabilities of the TGB_A. This operator is obtained from an approximation scheme which (1) neglects dislocation cores, (2) take the amplitude of the smectic order parameter to be fixed, and (3) coarse grains the resulting TGB_A stability operator, to remove the short wavelength (i.e., $l_b l_d$) spatial dependence.

Our analysis of these transitions begins with the London approximation which assumes that the dislocation core radius ($\sim\xi$) is smaller than the typical dislocation spacing l. In this case, we may divide the Gibbs energy into contributions associated with the dislocation core and the exterior environment,

$$G(n,\psi)=\sum_i G_{\rm core}(\hat{\mathbf{n}},\mathbf{R}_i(s))+G_{\rm ext}(\hat{\mathbf{n}},\psi)\ , \tag{38}$$

where $\mathbf{R}_i(s)$ is the coordinate of the ith dislocation. $G_{\rm core}$ includes the core contributions to the dislocation line tension and curvature energies. However we can, in fact, ignore the core energy near the Sm-A–Sm-C and TGB_A-TGB_C phase boundaries (where κ is large) because they are much smaller than the exterior energy.

Before we can give a more explicit expression for G, we need to introduce some notation which will be useful in characterizing unit-vector fields, such as the director $\hat{n}$ and the layer normal $\hat{N}$. If $\hat{V}(\mathbf{r})$ is such a vector, we may write

$$\hat{V}(\mathbf{r})=(1-V_x^2)^{1/2}(0,\cos(\bar{k}_0 x+\phi_V),\sin(\bar{k}_0 x+\phi_V))+V_x\hat{\mathbf{x}} \tag{39}$$

where $\bar{k}_0$ is the mean twist of the TGB. We will call ϕ_V the phase lag of $\hat{\mathbf{V}}$ and $\mathbf{\Phi}_V\equiv(\phi_V,V_x)$ the phase-lag components of $\hat{\mathbf{V}}$.

With this new notation, we now consider the detailed form of G. In accordance with our approximation scheme, we drop $G_{\rm core}$ and observe that $G\approx G_{\rm ext}(n,\psi)$ consists of contributions from both $F_{\rm CL}$, $F_{\rm Frank}$, and the chirality term. To calculate the contribution of $F_{\rm CL}$ we take $|\psi(\mathbf{r})|=\psi_0$. This gives

$$F_{\rm CL}=\int d^3r\,[\tfrac{1}{2}\mathbf{v}_s\cdot\mathbf{\Delta}_\psi(\nabla,\mathbf{r})\cdot\mathbf{v}_s+g_\psi\mathbf{v}_s^4+(r|\psi|^2+g|\psi|^4)]\ , \tag{40}$$

where $\mathbf{v}_s=\mathbf{\Phi}_n-\mathbf{\Phi}_\kappa$,

$$g_\psi=D_\perp\psi_0^2q_0^4\left[1+\frac{C_\parallel}{4D_\perp q_0^2}\right]\ ,$$

and

$$\Delta_\psi(\nabla,x)=\rho_s I+2D_\perp\psi_0^2q_0^2\begin{bmatrix}-\partial_x^2 & -\partial_x\hat{\mathbf{e}}_0\cdot\nabla\\ -\hat{\mathbf{e}}_0\cdot\nabla\partial_x & -\nabla\cdot\hat{\mathbf{e}}_0\hat{\mathbf{e}}_0\cdot\nabla\end{bmatrix}\ , \tag{41}$$

where $\hat{\mathbf{e}}_0\equiv(0,-\sin(k_0x),\cos(k_0x))$, $\hat{\mathbf{n}}_0\equiv(0,\cos(k_0x),\sin(k_0x))$, and where $\rho_s\equiv C_\perp\psi_0^2q_0^2$. Note that ρ_s changes sign at the Sm-A–Sm-C transition. Next we expand $F_{\rm Frank}$ in powers of Φ_n,

$$F_{\rm Frank}-h\int d^3r\,\hat{\mathbf{n}}\cdot\nabla\times\hat{\mathbf{n}}=\int d^3r\,[\tfrac{1}{2}\mathbf{\Phi}_n\cdot\mathbf{\Delta}_{\rm Frank}\cdot\mathbf{\Phi}_n+g_f\Phi_{nx}^4+(\tfrac{1}{2}K_2k_0^2-hk_0)]\ , \tag{42}$$

where

$$\tfrac{1}{2}\Delta_{\text{Frank}}(\nabla,x)\equiv\begin{bmatrix} -\nabla\cdot\dfrac{1}{2M_x(x)}\cdot\nabla+\rho_{\text{ani}} & \tilde{h}(\hat{\mathbf{n}}_0\cdot\nabla)-\tfrac{1}{2}(K_1-K_2)(\hat{\mathbf{e}}_0\cdot\nabla)\partial_x \\ \text{H.c.} & -\nabla\cdot\dfrac{1}{2M_\phi(x)}\cdot\nabla \end{bmatrix} \tag{43}$$

with

$$-\nabla\cdot\frac{1}{2M_x(x)}\cdot\nabla\equiv-\tfrac{1}{2}K_1\partial_x^2-\tfrac{1}{2}\nabla\cdot(K_3\hat{\mathbf{n}}_0\hat{\mathbf{n}}_0+K_2\hat{\mathbf{e}}_0\hat{\mathbf{e}}_0)\cdot\nabla\ , \tag{44}$$

$$-\nabla\cdot\frac{1}{2M_\phi(x)}\cdot\nabla\equiv-\tfrac{1}{2}K_2\partial_x^2-\tfrac{1}{2}\nabla\cdot(K_3\hat{\mathbf{n}}_0\hat{\mathbf{n}}_0+K_1\hat{\mathbf{e}}_0\hat{\mathbf{e}}_0)\cdot\nabla\ , \tag{45}$$

and where $\tilde{h}=h-K_2k_0+\frac{1}{2}(K_1+K_3)k_0$ and $\rho_{\text{ani}}=\tilde{h}k_0/2$. This expansion of F_{Frank} should be quite reliable near $C_\perp=0$, since Φ_n, the deviation of $\hat{\mathbf{n}}$ from a uniformly twisting state, vanishes as dl/λ^2. One should also note that the derivation of the above expressions did not assume $k_0=k_{N^*}$ $(=h/K_2)$ as would be the case in the absence of layering.

There are two additional features of $\Delta_{\text{Frank}}(\nabla,x)$ which are also worth noting. The first is Δ_{Frank}'s long-wavelength limit. In this limit, the (ϕ,ϕ) component of $\Delta_{\text{Frank}}(\nabla,x)$ vanishes but the (x,x) component does not. This is significant. The vanishing (ϕ,ϕ) component reflects the fact that $\delta\Phi=(0,1)$ is a rotation of the director configuration, about the pitch axis, which costs no energy. By comparison, the nonvanishing (x,x) component $(=\rho_{\text{ani}})$ suppresses deviations of the cholesteric director out of the plane perpendicular to the pitch axis. The second notable feature of Δ_{Frank} is the off-diagonal terms $\tilde{h}(\hat{\mathbf{n}}_0\cdot\nabla)$. Under appropriate circumstances, they cause Φ_n to locally precess about the cholesteric director field $\hat{\mathbf{n}}_0$ as one moves along the $\hat{\mathbf{n}}_0(\mathbf{r})$ direction. When $k_0=0$, this effect is responsible for producing a Sm-C^*. However, if $k_0\neq0$, it will favor Sm-C^* over Sm-C-like TGB slabs.

Now combining F_{CL} with $F_{\text{Frank}}-h\hat{\mathbf{n}}\cdot\nabla\times\hat{\mathbf{n}}$ gives

$$G_{\text{ext}}=F(k_0)+\int d^3r\,[\tfrac{1}{2}\Phi_n\cdot\Delta_{\text{Frank}}(\nabla,x)\cdot\Phi_n+\tfrac{1}{2}\mathbf{v}_s\cdot\Delta_\psi(\nabla,x)\mathbf{v}_s+g_f\Phi_{nx}^4+g_\psi\mathbf{v}_s^4]\ , \tag{46}$$

where $g_f\equiv\frac{1}{2}(K_2-K_3)k_0^2$ and $F(k_0)\equiv\frac{1}{2}K_2k_0^2-hk_0+r|\psi_0|^2+g|\psi_0|^4$. Now assuming that the chirality is sufficiently small and noting that $|r|<|r_{c1}|\to0$ as $h\to0$, we have $|r|\ll gK_1/(D_\perp q_0^4)$. In this case, Eq. (46) simplifies to

$$G_{\text{ext}}\approx\int d^3r\,[\tfrac{1}{2}\Phi_n\cdot\Delta_{\text{Frank}}\cdot\Phi_n+\tfrac{1}{2}\rho_s\mathbf{v}_s^2+(g_f\Phi_{nx}^4+g_\psi v_s^4)]\ , \tag{47}$$

Where we redefined the zero of energy to suppress $F(k_0)$. The quadratic part of this expression should be compared to the free energy of a superconductor, i.e.,

$$G=\int d^3r\left[\frac{1}{8\pi\mu_0}(\nabla\times\mathbf{A})^2+\frac{1}{4\pi\mu_0}\mathbf{H}_{\text{ext}}\cdot\nabla\times\mathbf{A}+\tfrac{1}{2}\rho_s\mathbf{v}_s^2\right]\ , \tag{48}$$

where ρ_s is the superfluid density and where $\mathbf{v}_s$ is the superfluid velocity. The latter is related to the order-parameter phase u by $\mathbf{v}_s\equiv\nabla u-2ie\,\mathbf{A}$. Comparing Eqs. (46) and (48), we see that the deviation of the director and the layer normal corresponds to the superfluid velocity $\mathbf{v}_s$.

Now we turn to our stability analysis of the TGB$_A$ near $C_\perp=0$. For simplicity, we will take the smectic order-parameter field to be held constant, so the stability kernel

$$\chi^{-1}(r,r')=\frac{\delta^2G}{\Phi_n(r)\Phi_n(r')}=[\Delta_{\text{Frank}}(\nabla,x)+\rho_sI]+12g_fn_x^2\delta_{ij}^{xx}+4g_\psi(2\delta_{ij}\mathbf{v}_s^2+v_{si}v_{sj})\ , \tag{49}$$

where $\delta_{ij}^{ab}=\delta_{ia}\delta_{bj}$. Unfortunately the spatial dependence of the g_f and g_ψ terms make $\chi^{-1}(r,r')$ into a type of quasiperiodic Schrödinger operator. To determine whether these contributions are significant, we compare them with all the various terms that appear in the matrix elements of Δ_{Frank} (e.g., ρ_{ani}, $K_2k_0q_c$, and $\frac{1}{2}K_3q_c^2$). Depending on the system parameters, these terms can be as large as $O(K_2k_0^2)$. By comparing the Δ_{Frank} terms with the g_f term [which is $\sim K_2k_0^2(k_0l)^2$], we see that the latter is smaller by a factor of $O((k_0l)^2)$. Moreover, one can verify that the g_f term produces a fractional shift in the TGB$_A$–TGB$_{C^*}$ line which is of order $O((k_0l)^2)$. Hence, this term is negligible. Next consider the g_ψ terms. These are of order $D_\perp\psi_0^2q_0^4(k_0l)^2$. Unlike the g_f term, they are not higher order in the expansion in powers of k_0 and, hence, will be included.

To at least partially take the g_ψ terms into account, we observe that the spatially dependent part of the g_ψ term oscillates with periods l_b and l_d. These periods ($\sim$200 Å) are much shorter than the length scales of interest [viz., the Sm-C^* slab width, and the cholesteric and Sm-C^* pitch lengths (>4500 Å)] [29]. The oscillations are, therefore, unlikely to have a significant effect. We will simply replace the g_ψ term by its spatial average. One may wish to think of this as a simple coarse-graining procedure. Using the D_q symmetry of the TGB$_A$, we can write the averaged g_ψ term as

$$2\delta_{ij}\langle\Phi^2\rangle+\langle\Phi_i\Phi_j\rangle=\tfrac{1}{4}[f_1\delta_{ij}+f_2(\sigma_z)_{ij}](k_0l)^2\ , \tag{50}$$

where $f_{1,2}(\rho_s,r_\psi)$ are slowly varying functions of order unity. For the purposes of our subsequent discussion, we will take f_1 and f_2 to be constant. The stability of the

TGB_A with respect to the TGB_C and TGB_{C^*} may, therefore, be studied using the approximate stability operator

$$\chi^{-1}(\nabla,x)=\begin{bmatrix}\chi_{xx}^{-1} & \chi_{x\phi}^{-1}\\ \chi_{\phi x}^{-1} & \chi_{\phi\phi}^{-1}\end{bmatrix} \approx \Delta'_{\mathrm{Frank}}(\nabla,x)+\rho'_s I \ , \tag{51}$$

where $\rho'_s\equiv\rho_s+(f_1-f_2)(k_0 l)^2$ and where Δ'_{Frank} is defined like Δ_{Frank} [see Eq. (43)] except with ρ_s and ρ_{ani} being replaced by ρ'_s and $\rho'_{\mathrm{ani}}\equiv\rho_{\mathrm{ani}}+f_2 g_\psi (k_0 l)^2$, respectively. The consequences of the coarse-grained stability operator will be explored in Sec. V C.

C. Transitions among the TGB phases within the coarse-grained theory

We will now begin the analysis of the coarse-grained theory by discussing the least stable modes. Translation invariance implies that these modes are of the form

$$\mathbf{\Phi}=\begin{bmatrix}n_x^0(x)\\ \phi^0(x)\end{bmatrix}\exp(i\mathbf{q}_\perp\cdot\mathbf{r})=\mathbf{\Phi}_0(x)\exp(i\mathbf{q}_\perp\cdot\mathbf{r}) \ , \tag{52}$$

where

$$\chi^{-1}(\partial_x,\mathbf{q}_\perp,x)\mathbf{\Phi}_0(x)=\lambda\mathbf{\Phi}_0(x) \ . \tag{53}$$

If the least stable mode has $q_\perp=0$ and $n_x=0$, then it describes the TGB_A-TGB_C transition. For $\mathbf{q}_\perp\neq\mathbf{0}$, the least stable mode describes the TGB_A-TGB_{C^*} transition. To understand why a $q_\perp=0$ instability corresponds to the formation of the TGB_{C^*}, we must first observe that $\chi^{-1}(\partial_x,\mathbf{q}_\perp,x+P)=\chi^{-1}(\partial_x,\mathbf{q}_\perp,x)$. This implies that the stability modes are Bloch functions, i.e., $\mathbf{\Phi}_0(x)=\exp(ikx)\mathbf{u}(x)$. For $q_\perp\neq0$, the barrier heights of the "potential" terms of $\chi^{-1}(\partial_x,q_\perp,x)$ will localize $\mathbf{u}(x)$ within a slab of width $\xi_H\sim\sqrt{2\pi P/q_\perp}$, inside the cholesteric unit cell $[0,P)$. This localized mode is the helislab which was discussed in Sec. IV.

To further simplify χ^{-1}, we will assume that $P_c/P\ll1$. But since pitch lengths of cholesterics tend to be smaller than the Sm-C^* pitch length, this may not appear to be a very physical limit. However, it does, in fact, hold near a continuous (or weakly first order) TGB_{C^*}–Sm-C^* transition since P diverges while P_c remains finite. Moreover, we will argue that the TGB_{C^*} does not exist if $P_c/P>O(1)$. Hence $P_c/P\ll1$, is indeed, the relevant limit. It is also a particularly simple limit, since the overlap of the wave function in adjacent cells is small $[\sim\exp-(P/P_c)]$. This, of course, means that the bandwidth of the least stable band collapses. So we may take the localized Wannier functions to be the least stable modes and calculate them by solving the eigenproblem with $M_{\mathrm{tot}}(\partial_x,x)$ expanded about the mode center. Let $\mathbf{q}_\perp=q\hat{\mathbf{n}}_0(\bar{x}=0)$, then for $x\approx0$ we have

$$\chi_{xx}^{-1}=-\nabla\cdot\frac{1}{2M_x(x)}\cdot\nabla+\rho_s \approx -\tfrac{1}{2}K_1\partial_x^2+\alpha(qk_0)^2x^2+\tfrac{1}{2}K_3q^2+2\rho'_{\mathrm{ani}}+\rho'_s \ , \tag{54}$$

$$\chi_{\phi\phi}^{-1}=-\nabla\cdot\frac{1}{2M_\phi(x)}\cdot\nabla+\rho_s \approx -\tfrac{1}{2}K_2\partial_x^2+\beta(qk_0)^2x^2+\tfrac{1}{2}K_3q^2+\rho_s \ , \tag{55}$$

and

$$\chi_{\phi x}^{-1}\approx -i\tilde{h}q[1-\tfrac{1}{2}(k_0q)^2]-(\alpha-\beta)iqk_0\partial_x x +O((k_0q)^3) \ , \tag{56}$$

where $\alpha\equiv\frac{1}{2}(K_2-K_3)$ and $\beta=\frac{1}{2}(K_1-K_3)$. Note that all these matrix elements are even in x which indicates that the slab is localized about $x=0$. This, in turn, means that at the center of the helislab, the helilayer normals are coaxial with the director precession cone. However, as one moves away from the helislab center, the layer normal and the director precession cone axis will no longer coincide. Of course, in an untwisted and unstrained Sm-C^*, the helilayer normal coincides with the precession cone axis everywhere. These remarks should suggest an interesting analogy between TGB_{C^*} helislabs and TGB_A smectic slabs. In particular, the director and the layer normal of the TGB_A slabs are analogs of the precession cone axis and the helilayer normal.

The above simplified form of $\chi^{-1}(\partial_x,x)$ may be thought of as a matrix version of the harmonic-oscillator Hamiltonian. Unfortunately, it does not appear possible to obtain the exact eigenfunctions analytically. In particular, the eigenfunctions are not Gaussian. Nevertheless, it is clear that if $q\neq0$ then the actual eigenstates of Eq. (53) are bound states so one may use

$$\mathbf{\Phi}_0(x)=\mathbf{u}_0N^{-1/2}\exp(-x^2/4\xi_H^2) \tag{57}$$

as a variational ansatz. This variational eigenfunction represents a TGB_{C^*} helislab of width ξ_H. In this helislab, an amplitude ($|\mathbf{c}|$) oscillation will coexist with the $\mathbf{c}$-director precession unless $u_x=iu_\phi$. If one thinks of the twisting $\mathbf{c}$ director in an undistorted Sm-C^* sample as being a circularly polarized waveform, then a state with $u_x\neq iu_\phi$ would look like an elliptically polarized waveform. The elliptical, rather than circular, precession is due to the Ising anisotropy discussed in Sec. V A. Now if we move deeper into the TGB_{C^*} phase, the elliptical precession of the $\mathbf{c}$ director would evolve as the director amplitude grows and saturates. Indeed, if one assumes that the $\mathbf{c}$ director amplitude is fully saturated, then the Ising anisotropy would produce a helislab consisting of a one-dimensional lattice of π walls separating distinct smectic-C-like regions (i.e., regions where $n_x^0\approx0$). However, such behavior is of little concern since we are restricting our analysis to the vicinity of the TGB_A-TGB_{C^*} phase boundary.

Now using the variational eigenfunction, we wish to determine the values of q and ξ_H which minimize $\langle M_0\rangle$. To do this, we need the smallest eigenvalue $\lambda(q)$ and the corresponding eigenvector $\mathbf{u}$ of

$$\underline{m}\equiv\underline{A}(k_0|q|)+\underline{B} \ , \tag{58}$$

where

$$\underline{A}=\begin{bmatrix} \frac{1}{8}K_1x+\dfrac{\alpha}{x} & i\left[\dfrac{\tilde{h}}{k_0}+\dfrac{\alpha-\beta}{2}\right]\mathrm{sgn}q \\ \text{c.c.} & \frac{1}{8}K_2x+\dfrac{\beta}{x} \end{bmatrix} \tag{59}$$

and

$$\underline{B}(q)=2\rho'_{\mathrm{ani}}\hat{\mathbf{x}}\hat{\mathbf{x}}+(\rho'_s+\tfrac{1}{2}K_3q^2)I\ , \tag{60}$$

and where x, defined by $\xi_H^{-2}\equiv xk_0|q|$, is not to be confused with the pitch axis coordinate.

We first observe that if either $K_1<K_3$ or $K_2<K_3$ then the eigenvalues of $\underline{m}$ are unbounded from below. This may been seen by taking $x\to 0$. Although our harmonic-oscillator approximation scheme breaks down for such large slabs, this nevertheless implies that the slab width ξ_H is much greater than $\sqrt{P_cP}$. We interpret this as indicating that the TGB_{C^*} is unstable with respect to TGB_C.

To simplify the remaining discussion of the eigenvalues $\lambda_\pm(q)$, let $K_1=K_2\equiv K$. Then the eigenvalues become

$$\lambda_\pm(q)=\left[\tfrac{1}{8}Kx+\frac{\alpha}{x}\right]k_0|q|+(\rho'_s+\tfrac{1}{2}K_3q^2)+\rho'_{\mathrm{ani}}\pm[(\rho'_{\mathrm{ani}})^2+(\tilde{h}q)^2]^{1/2}\ . \tag{61}$$

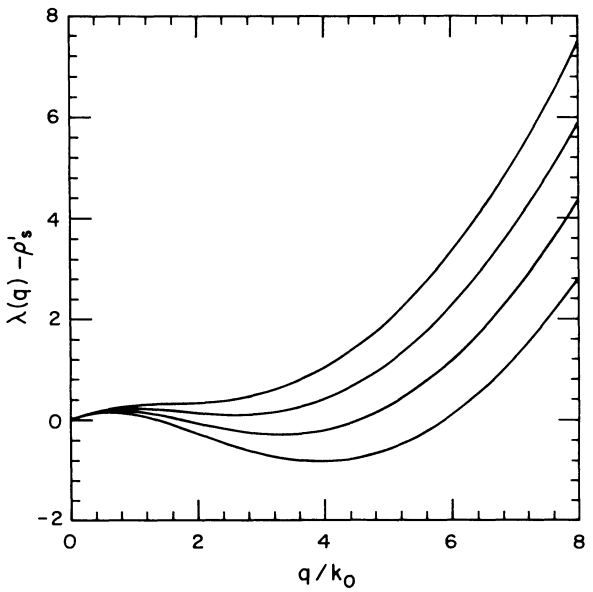

FIG. 10. A plot of $\lambda(q)_-$, the least stable eigenvalue branch assuming $\sqrt{K(K-K_3)}=2K_3$ for $\tilde{h}/(K_3k_0)=4.0$, 4.5, 5.0, and 5.5. For the $\tilde{h}/(K_3k_0)=4.0$ and 4.5, the minimum occurs at $q_{\min}\neq 0$ which corresponds to a TGB_A-TGB_{C^*} transition. However, for $\tilde{h}/K_3k_0\gtrsim 5$, the TGB_A-TGB_{C^*} mode with $q_{\min}\neq 0$ becomes unstable before the TGB_A-TGB_C mode with $q=0$. Typically the TGB_A-TGB_{C^*} transition preempts the TGB_A-TGB_C transition when P_c/P is sufficiently small. This theory describes a bicritical point where the TGB_A-TGB_C and the second-order TGB_A-TGB_{C^*} meet a first-order TGB_C-TGB_{C^*}.

Minimizing λ_- with respect to x, we obtain x and the helislab width

$$\xi_H=2\left[\frac{K}{(K-K_3)(qk_0)}\right]^{1/2}\ . \tag{62}$$

Now, given this ξ_H, we wish to minimize $\lambda_-(q)$ with respect to q. (See Fig. 10.) To do this observe that

$$\lambda_-(q)\approx\begin{cases} \frac{1}{2}\sqrt{K(K-K_3)}k_0|q|-\tilde{h}|q|+(\rho'_s+\rho'_{\mathrm{ani}}) \\ \qquad +\frac{1}{2}K_3q^2 \quad \text{if } q>\frac{1}{2}k_0 \\ \frac{1}{2}\sqrt{K(K-K_3)}k_0|q|+\rho'_s+O(q^2) \\ \qquad \text{if } q<\frac{1}{2}k_0\ . \end{cases} \tag{63}$$

So

$$q_{\min}\approx\begin{cases}[\tilde{h}-\frac{1}{2}\sqrt{K(K-K_3)}k_0]/K_3 & \text{if } q_{\min}>\frac{1}{2}k_0 \\ 0, \quad \text{otherwise}\ . \end{cases} \tag{64}$$

We see that a discontinuous change from the $q\neq 0$ instability to the $q=0$ instability occurs for $k_0\approx 2q_{\min}$. This allows us to estimate the critical cholesteric twist k_f^0 above which the Sm-C^* modulation is expelled. We find $k_c^0=2h/3K=2k_{N^*}/3$ to within corrections of order $O(K_3/K)$. These results imply that if $K_3<K$ then (1) the TGB_C separates the cholesteric from the TGB_{C^*} and that (2) a first-order TGB_C-TGB_{C^*} transition line, the second-order TGB_A-TGB_C line, and the second-order TGB_A-TGB_{C^*} lines intersect at a bicritical point. (See Figs. 11 and 12.)

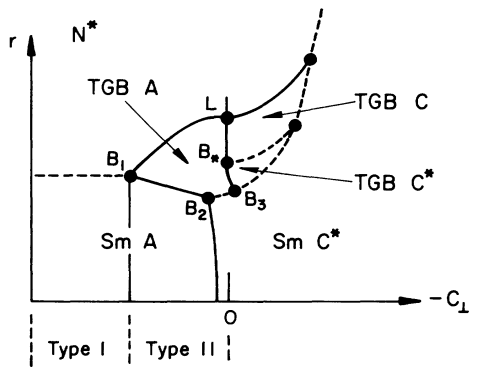

FIG. 11. The phase diagram of the chiral Chen-Lubensky model [i.e., of $F_{\mathrm{CL}}=F_{\mathrm{de\,Gennes}}+F_D+F_{\mathrm{Frank}}$, defined by Eqs. (2)–(5)] when K_1 and $K_2>K_3$. The TGB_A, TGB_C, and TGB_{C^*} phases are grain-boundary phases consisting of stacks of Sm-A, Sm-C, and Sm-C^* slabs, respectively. In type-I liquid crystals, the N^*–Sm-A transition is first order. In type-II liquid crystals, the TGB_A phase intervenes between the N^* and Sm-A phases. From the Sm-C^* phase, one can enter either the TGB_A, TGB_C, or the TGB_{C^*} phase. The TGB_A-TGB_C transition is a second-order Ising-like transition which spontaneously breaks the D_q symmetric TGB_A phase to a C_q symmetric TGB_C phase. The TGB_C-TGB_{C^*} phase is first order near the TGB_A-TGB_C-TGB_{C^*} bicritical point. The N^*-TGB_A and the N^*-TGB_C phases are second order.

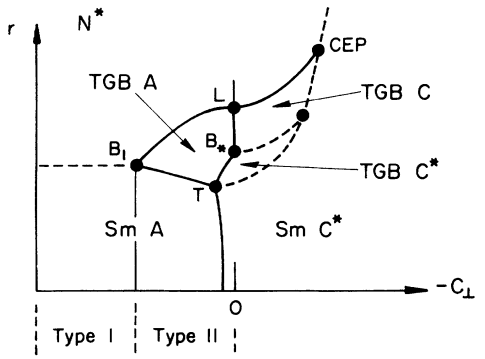

FIG. 12. Same as in Fig. 11, except assuming a long-range repulsive interaction between dislocations which is proportional to $1/r^{\beta}$ with $\beta>1$. The TGB_A-TGB_{C*} line is now cotangent to the Sm-A-Sm-C^* phase boundary, which eliminates the TGB_A-Sm-C^* segment of the H_{c1}.

Next we consider the positions of the TGB_A-TGB_C and TGB_A-TGB_{C*} phase boundaries. By setting $\lambda_-(q=0)=0$ one finds that the TGB_A-TGB_C phase boundary is

$$C_\perp = -\text{const}\times\left[1+\frac{C_\parallel}{4D_\perp q_0^2}\right]D_\perp k_0 q_0 , \tag{65}$$

where the constant is positive and proportional to f_1-f_2. For small k_0, this lies in a rather narrow strip, about the Sm-A-Sm-C phase boundary (i.e., $C_\perp=0$). To within the accuracy of the formulas, the TGB_A-TGB_C phase boundary together with the two H_{c1} lines intersect at (presumably) a Liftshitz point located at

$$(C_\perp, r)\sim -(A_1 D_\perp k_0 q_0, A_2 D_\perp q_0^2 k_0^2) .$$

A_1 and A_2 are expressions, of order unity, which depend on $C_\parallel/4D_\perp q_0^2$.

We can, now, draw a complete phase diagram when either $K_1<K_3$ or $K_2<K_3$. See Fig. 13. Note that the TGB_A-TGB_C and the Sm-A–Sm-C^* lines intersect the H_{c1} line at different points. This indicates that a segment

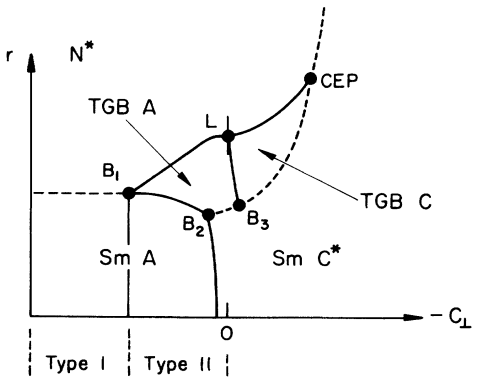

FIG. 13. Same as in Fig. 11 except with K_1 and $K_2<K_3$. On the Sm-C* side of the phase diagram, the TGB_{C*} phase no longer occurs.

of the H_{c1} line is a first-order TGB_A-Sm-C^*-phase boundary.

To complete the phase diagram for $K_1=K_2>K_3$, we must find the TGB_A-TGB_{C*} line. Let $\rho_*(r_\psi)$ denote the value of ρ_s at this line. Then using Eq. (64) for $q_{\min}$ and setting $\lambda_-(q)=0$ we get

$$\rho_* = -\rho_{\text{ani}} + \frac{1}{2K_3}[\tilde{h} - \tfrac{1}{2}\sqrt{K(K-K_3)}k_0]^2 - f_2(k_0 l)^2 . \tag{66}$$

Unfortunately, without a detailed equation of state [i.e., $k_0(h)$] near the TGB_A-TGB_{C*} border, this result has only limited value. One can, however, use it to obtain the structure of the multicritical points near T, the intersection of the H_{c1} lines with the Sm-A-Sm-C^* line. To do this we rewrite Eq. (66) as

$$\rho_s = \left[\frac{h^2}{2K_3} - \left[\frac{K}{K_3}+\frac{\sqrt{K(K-K_3)}}{2K_3}\right]hk_0\right] \times L\left[\frac{C_\perp}{D_\perp q_0 k_0}, \frac{C_\parallel}{4D_\perp q_0^2}\right] + O(k_0^2) , \tag{67}$$

where $L(x,y)\equiv[1+\text{const}\times f_1(1+y)/x]^{-1}$. This indicates that the TGB_A-TGB_{C*} line is on the C side of the Sm-A-Sm-C^* phase boundary. The latter is given by $\rho_{A\text{-}C}=h^2/(2k_3)$. One can now use the equation of state

$$k_0 = \frac{d}{\lambda^2}\left[\ln\left[\frac{l_d}{\lambda}\frac{K_2 d}{2(h-h_{c1})\lambda^2}\right] \times \ln\left[\frac{l_b}{l_d}\frac{K_2 d}{2(h-h_{c1})\lambda^2}\right]\right] \tag{68}$$

which can be derived in the $l_b, l_d \gg \lambda$ limit [see Eq. (95)]. One thereby obtains an explicit form to the TGB_A-TGB_{C*} boundary near the H_{c1} line

$$r_*(C_\perp) - r_{c1}(C_\perp) \sim \exp-\left[\frac{C_\perp \lambda_1^2/(f_1 d)}{[r_{c1}(C_\perp)-r_{A\text{-}C}(C_\perp)]^{-1/2}}\right] . \tag{69}$$

Combining this with the observation that $r_{c1}-r_{A\text{-}C}$ vanishes as T is approached, we conclude that the TGB_A-TGB_{C*} and the TGB_A-Sm-A lines are cotangent.

Next we observe that the h_{c1} line is also cotangent to the TGB_A-Sm-A line. The question, therefore, arises whether the TGB_A-TGB_{C*} lies above or below the h_{c1} line in the immediate neighborhood of T. The answer depends on the TGB_C-Sm-C^* line. If a segment of the h_{c1} line lies above the TGB_A-TGB_{C*} line, then the h_{c1} segment would be a first-order TGB_A-Sm-C^* transition line. (See Fig. 11.) As one moves into the TGB_A, across such a first-order TGB_A-Sm-C^* line, ordinary and helidislocations are spontaneously generated. However, the dislocations would collapse to the TGB_A with a finite $(l_b, l_d \sim \lambda)$ spacing, destroying both the Sm-C^* and Sm-C ordering in the process. If, however, the h_{c1} line is below

the TGB_A-TGB_C line, then one no longer has a pair of bicritical points separated by a first-order line. Instead one has a tetracritical point where the two H_{c1} lines (the TGB_{C^*}–Sm-C^* and the TGB_A–Sm-A), the Ising-like TGB_A-TGB_{C^*}, and the xy-like Sm-A–Sm-C^* intersect. (See Fig. 12.) One can apply similar arguments to conclude that a first-order TGB_A–Sm-A would also split the tetracritical point either into a pair of critical end points (CEP) or a CEP and a bicritical point.

VI. CONCLUSIONS

We have largely completed the phase diagram of the chiral Chen-Lubensky model. The principle results are summarized in Figs. 11–13. The basic results are as follows: We have shown that the Sm-C^* phase can exhibit transitions to the TGB_A, TGB_C, or TGB_{C^*}. In addition, we find that both the N^*-TGB_A and N^*-TGB_C transitions are possible, but that the N^*-TGB_{C^*} does not occur. In our discussion of the TGB_A-TGB_C and TGB_A-TGB_{C^*} transitions, we argued that the D_q symmetric TGB_A would exhibit an Ising-like transition to the C_q symmetric TGB_C. We also showed that the TGB_A-TGB_C is replaced by the TGB_A-TGB_{C^*} transition when the cholesteric pitch length P increases beyond $\sim 2P_c/3$, where P_c is the Sm-C^* pitch length.

In spite of these results the chiral N-A-C phase diagrams are incomplete in several respects. First, we have not located the intersection of the TGB_C-TGB_{C^*} and H_{c1} lines. In addition, we do not know whether there exists a tricritical point on the TGB_C-TGB_{C^*} line. (Although we showed that this line was first order near the TGB_A-TGB_C-TGB_{C^*} bicritical point, one could easily imagine that the transition becomes second order once the amplitude of the **c** director saturated.) In particular, one could imagine a TGB_C-TGB_{C^*} transition where P_c diverges like the soliton spacing in the Frank–van der Meer model during an incommensurate-commensurate transition [30].

Of course the most notable result of this study is the existence of the two new phases, the TGB_C and the TGB_{C^*}. (The latter occurs only when K_1 and $K_2 < K_3$.) At the time of writing, these phases have not been observed. Of course, if the new phases were found they would be distinguishable from the TGB_A by the existence of short-range Sm-C ordering (detectable by x-ray scattering). However, one could not necessarily distinguish the phases optically since the optical properties of the TGB_C would be quite similar to the TGB_A. By contrast, the optical properties of the TGB_{C^*} should be quite distinct from both the TGB_A and TGB_C. In particular, one might hope to observe, in the TGB_{C^*}, an optical analog of the TGB Bragg cylinder. It is hoped that this work will inspire experimentalists to hunt for these new phases.

ACKNOWLEDGMENTS

The author would like to thank Tom Lubensky, Ming Huang, David Mermin, Jay Patel, and John Toner for helpful discussions. He would also like to acknowledge support from the John and Lucille Packard Foundation (Grant No. FDN 89-1606).

APPENDIX A: GROUP THEORETICAL CONSTRAINTS ON THE TGB_A-TGB_{C^*} TRANSITION

In this appendix we wish to consider the consequences of the macroscopic TGB symmetry on the TGB_A-TGB_C transition. We begin our discussion by defining the point-group operators d_y and $\mathcal{R}_\theta$ in terms of their action on the director and smectic order-parameter fields,

$$d_y\hat{\mathbf{n}}(\mathbf{r}) \equiv (-n_x(d_y\mathbf{r}), n_y(d_y\mathbf{r}), -n_z(d_y\mathbf{r})) \equiv R^{-1}(d_y)\mathbf{n}(d_y\mathbf{r}) , \tag{A1}$$

$$d_y\psi(\mathbf{r}) \equiv \psi(d_y\mathbf{r}) \tag{A2}$$

and

$$\mathcal{R}_\theta\hat{\mathbf{n}}(\mathbf{r}) \equiv R_\theta^{-1}\hat{\mathbf{n}}(R_\theta r) , \tag{A3}$$

$$\mathcal{R}_\theta\psi(\mathbf{r}) \equiv \psi(R_\theta\mathbf{r}) , \tag{A4}$$

where R_θ is the matrix which rotates vectors by an angle θ about the pitch axis and where $d_y\mathbf{r}=(-x,y,-z)$. However, for the following discussion, it is convenient to define d_y and $\mathcal{R}_\theta$ in terms of their action on the phase lag components of $\hat{\mathbf{n}}$,

$$d_y\Phi_n(\mathbf{r}) \equiv -(\phi_n(d_y\mathbf{r}), n_x(d_y\mathbf{r})) \equiv D_0^{-1}(d_y)\Phi(d_y\mathbf{r}) , \tag{A5}$$

$$\mathcal{R}_\theta\Phi_n(\mathbf{r}) \equiv (\phi_n(R_\theta\mathbf{r})+\theta, n_x(R_\theta\mathbf{r})) \equiv D_0^{-1}(R_\theta)\Phi(R\mathbf{r})+(\theta,0) , \tag{A6}$$

where $D_0(\mathcal{R}_\theta)\equiv I$ and $D_0(d_y)\equiv -I$ define a representation of D_∞.

Next consider the stability kernel $\chi^{-1}(r,r')$ of the TGB_A phase with order parameter $\psi_0(\mathbf{r})$ and director field $\Phi_0(\mathbf{r})$,

$$\chi^{-1}(\mathbf{r},\mathbf{r}') \equiv \begin{bmatrix} \chi^{-1}_{\Phi_0\Phi_0} & \chi^{-1}_{\Phi_0\psi_0} \\ \chi^{-1}_{\psi_0\Phi_0} & \chi^{-1}_{\psi_0\psi_0} \end{bmatrix} , \tag{A7}$$

where

$$\chi^{-1}_{\psi_0\psi_0} \equiv \frac{\delta^2 F}{\delta\psi_0(\mathbf{r})\delta\psi_0(\mathbf{r}')} , \tag{A8}$$

etc. Below we will prove that, if the macroscopic properties of the TGB_A phase are invariant under some point-group symmetry, then

$$\chi^{-1}_{\Phi\Phi}(gk,gk') = [D_0(g)\chi^{-1}_{\Phi\Phi}(k,k')D_0^{-1}(g)]e^{i\theta_g(k-k')} , \tag{A9}$$

$$\chi^{-1}_{\Phi\psi}(gk,gk') = D_0(g)\chi^{-1}_{\Phi\psi}(k,k')e^{i\theta_g(k-k')} , \tag{A10}$$

and

$$\chi^{-1}_{\psi\psi}(gk,gk') = \chi^{-1}_{\psi\psi}(k,k')e^{i\theta_g(k-k')} , \tag{A11}$$

where $\theta_g(k)$ is a phase transition which may be calculated from ψ_0 and Φ_0.

To prove the above identities, we first observe that the invariance of F under a point-group element g implies

$$F[\Phi_n(k),\psi(k)]=F[D_0^{-1}(g)\Phi_n(gk),\psi(gk)] =F[D_0^{-1}(g)\Phi_n(gk)e^{-i\theta_g(k)},\psi(k)] , \tag{A12}$$

where the last identity is valid for any $\theta_g(k)$ which is linear in K over the reciprocal lattice of (Φ,ψ). Note that (A12) is valid independent of the form of ψ and Φ. Now since ψ_0 and Φ_0 describe a phase with the macroscopic D_q symmetry, one can readily show [19]

$$\psi(gk)=\psi(k)e^{i\theta_g(k)} \tag{A13}$$

and

$$R^{-1}(g)\hat{\mathbf{n}}(gk)=\hat{\mathbf{n}}(k)e^{i\theta_g(k)} , \tag{A14}$$

or equivalently

$$D_0^{-1}(g)\Phi_n(gk)=\Phi_n(k)e^{i\theta_g(k)} . \tag{A15}$$

In the above results, the phase function $\theta_g(k)$ is (1) linear in k, (2) defined on all reciprocal-lattice vectors, and (3) satisfies the group compatibility conditions: $\theta_{g_1g_2}(k)=\theta_{g_1}(g_2k)+\theta_{g_2}(k)$. In general, the phase function will depend on both the space group of (ψ_0,Φ_0) as well as the phonon-phason configuration. If we now twice functionally differentiate Eq. (A12) about ψ_0 and Φ_0 one obtains Eqs. (A9)–(A11).

Next we consider the eigenfunctions of χ^{-1}. Let

$$\int d^3\mathbf{r}'\chi^{-1}(r,r')\mathbf{V}_\alpha(\mathbf{r}')=\lambda\mathbf{V}_\alpha(\mathbf{r}) , \tag{A16}$$

where $\mathbf{V}_\alpha(r)$ $(\alpha=1,\ldots,D)$, are a degenerate set of $D\geq 1$ least stable eigenmodes, and let $\chi^{-1}(k,k')$ be the Fourier transform of $\chi^{-1}(r,r')$. Then the quasiperiodicity of $\psi(r)$ implies that $\chi^{-1}(k,k')$ vanishes unless $k-k'\in L$, the TGB_A reciprocal lattice. Consequently we can write the mode as a Bloch function

$$\mathbf{V}_\alpha(r)=e^{i\mathbf{k}_\alpha\cdot r}\sum_{G\in L}\mathbf{V}_\alpha(k+G)e^{i\mathbf{G}\cdot\mathbf{r}} , \tag{A17}$$

where $\sum_G|V(k+G)|^2$ will be finite if the mode is extended, and diverges if the mode is localized. In general, the set of vectors $\{\mathbf{k}_\alpha,\ \alpha=1,\ldots,D\}$ is symmetric under the point group D_q.

Observe that Eqs. (A2), (A4)–(A6), together with the Fourier transform of Eq. (A16), i.e.,

$$\sum_{G'\in L}\chi^{-1}(g(k+G),g(k+G'))\mathbf{V}_\alpha(g(k+G')) =\lambda\mathbf{V}_\alpha(g(k+G)) , \tag{A18}$$

imply

$$\sum_{G'\in L}\chi^{-1}(k+G,k+G') \times[D^{-1}(g)\mathbf{V}_\alpha(g(k+G'))]e^{-i\theta_g(k+G')} =\lambda[D^{-1}(g)\mathbf{V}_\alpha(g(k+G))]e^{-i\theta_g(k+G)} , \tag{A19}$$

where

$$D^{-1}(g)\equiv\begin{bmatrix}D_0^{-1}(g) & 0\\ 0 & I\end{bmatrix} . \tag{A20}$$

Hence, the eigenbasis transforms according to an irreducible representation of the (generally nonsymmorphic) space group, i.e.,

$$D_0^{-1}(g)\Phi_\alpha(gk)=\exp[i\theta_g(k)]\sum_\beta\Gamma_{\alpha\beta}(g)\Phi_\beta(k) \tag{A21}$$

and

$$\psi_\alpha(gk)=\exp[i\theta_g(k)]\sum_\beta\Gamma_{\alpha\beta}(g)\psi_\beta(k) , \tag{A22}$$

where $\mathbf{V}(k)\equiv(\Phi_\alpha,\psi_\alpha(k))$ are the director and order-parameter components of the stability mode, and where the matrices $\Gamma(g)$ form some irreducible representation of D_q.

It will be useful to have the explicit form of the representation matrices $\Gamma(g)$ for the group generators d and $\mathcal{R}_q$. The one-dimensional representations of D_q are listed in Table II. There are either $q-1$ or $q-2$ two-dimensional representations of D_q if q is odd or even, respectively. These are [31] E_l, with $l=1,2,\ldots,q-1$ or E_l, with $l=1,2,\ldots,(q/2)-1,(q/2)=1$ for q odd or even (respectively). A simple form of the E_l representation is given by the following matrices:

$$\Gamma_{E_l}(\mathcal{R})=\begin{bmatrix}\exp(2\pi il/q) & 0\\ 0 & \exp(-2\pi il/q)\end{bmatrix} \tag{A23}$$

and

$$\gamma_{E_l}(d)=\begin{bmatrix}1 & 0\\ 0 & 1\end{bmatrix} . \tag{A24}$$

With the above results, we can now investigate the ramifications of the D_q symmetry on the TGB_A-TGB_C transition. Near the transition

$$\Phi(\mathbf{r})=\Phi_0(\mathbf{r})+\sum_\alpha a_\alpha\Phi_\alpha(\mathbf{r}) , \qquad \psi(\mathbf{r})=\psi_0(\mathbf{r})+\sum_\alpha a_0\psi_\alpha(\mathbf{r}) , \tag{A25}$$

where ψ_0 and Φ_0 are the smectic order parameter and the director field of the TGB_A. Now Eqs. (A12), (A21), (A22), and (A25) imply that $F[a_\alpha]\equiv F[\Phi,\psi]$ equals $F(\sum a_\beta\Gamma_{\beta\alpha}(g))$. These point-group symmetry conditions are identical to conditions familiar from the theory of phase transitions occurring in systems with symmorphic space groups.

Using the explicit form of the Γ_{E_l} matrices, one may readily show that the Landau expansion contains no odd terms for any of the E representation order parameters.

TABLE II. The group characters for the representations of D_q. There are two or four one-dimensional representations for q odd or q even, respectively. The representations for q-odd representations are given in (a) and the q-even representations are given in (b). In both tables, $C(g)$ denotes the class containing the group element g. The group characters for the higher (i.e., two-) dimensional representations are not needed for the discussion in the text and have, therefore, been omitted.

(a) q odd

	$C(I)$	$C(r_q)$	$C(r_q^2)$	...	$C(r_q^{q/2})$	$C(d_y)$
A_1	1	1	1	...	1	1
A_2	1	1	1	...	1	-1

(b) q even

	$C(I)$	$C(r_q)$	$C(r_q^2)$	...	$C(r_q^{q/2-1})$	$C(r_q^{q/2})$	$C(d_y r_q^{2j})$	$C(d_y r_q^{2j+1})$
A_1	1	1	1	...	1	1	1	1
A_2	1	1	1	...	1	1	-1	-1
B_1	1	-1	1	...	$(-1)^{q/2-1}$	$(-1)^{q/2}$	1	-1
B_2	1	-1	1	...	$(-1)^{q/2-1}$	$(-1)^{q/2}$	-1	1

Moreover, inspection of Table II quickly reveals that only a Landau theory corresponding to a transition described by the A_1 representation (no-symmetry breaking) can exhibit a Landau expansion with odd terms. However, the A_1 representation is ruled out since the TGB_A-TGB_C transition breaks dihedral symmetry.

From the above discussion, we see that mean-field theory will predict a second or a first-order transition depending on the nature of the quartic terms. However, in the limit of large pitch (i.e., $P \gg l$), the quartic terms reduce to those describing the Sm-A–Sm-C transition. Therefore, in that limit, we predict that the TGB_A-TGB_C and TGB_A-TGB_{C^*} will be of the same order as the Sm-A–Sm-C and Sm-A–Sm-C^* transitions, respectively.

Finally, we wish to determine which representations of D_q describe a possible TGB_A-TGB_C order parameter. Only the A_2 and E_l ($l=1,\ldots$) representations break all of the dihedral symmetries necessary (and sufficient) to be TGB_A-TGB_C order parameters. Of course, these choices describe rather different transitions. In particular, the A_2 describes a transition to a TGB_C phase with C_q symmetry, whereas the E_l representations describe transitions to TGB_C phases with $C_{q'}$ symmetry, where $q=nq'$ for some integer $n>1$. In the Secs. V B and V C, we constructed a mean-field theory of the TGB_A-TGB_C and TGB_A-TGB_{C^*} transitions from the de Gennes model. That theory described a TGB_A-TGB_C transition with an order parameter transforming according to the A_2 representation.

APPENDIX B: MEAN-FIELD EQUATIONS OF STATE FOR THE TGB_A

We wish to calculate the twist as a function of chirality [i.e., $k_0(h)$] using a London approximation. The interaction energy for screw dislocations may be calculated within the de Gennes theory for untwisted smectics linearized about $\hat{\mathbf{n}} \approx \hat{\mathbf{z}}$. This has been done by Day, Lubensky, and McKane [32]. They found, in the absence of chirality, that

$$F_{\mathrm{int}} = \frac{1}{(2\pi)^2} \int d^2\mathbf{q}\, \mathbf{m}(-q) \cdot \underline{U}(q) \cdot \mathbf{m}(q) \ , \tag{B1}$$

where

$$\underline{U}(q) = U_c(q) \hat{\mathbf{e}}_t \hat{\mathbf{e}}_t + U_s(q) \hat{\mathbf{e}}_\perp \hat{\mathbf{e}}_\perp$$

with

$$U_s(q) = \frac{1}{q^2} \frac{K_2 q_2^2 + K_3 q_1^2}{\lambda_2^2 q_2^2 + \lambda_3^2 q_1^2 + 1} \ , \tag{B2}$$

$$U_e(q) = \frac{K_1 (q_2/q_1)^2 + K_3}{[K_1 (q_2/q_1)^2 + K_3 q^2] + 1} \ , \tag{B3}$$

$\hat{\mathbf{e}} = \hat{\mathbf{n}}_0 \times \mathbf{q} / |\hat{\mathbf{n}}_0 \times \mathbf{q}|$, and $\hat{\mathbf{e}}_\perp = \mathbf{q} \times \hat{\mathbf{e}}_t / |\mathbf{q} \times \hat{\mathbf{e}}_t|$. The above expressions are defined for a coordinate system where $\hat{\mathbf{n}}_0$ point along the 1 direction and $\mathbf{q}$ lies in the 1-2 plane. Adding the contribution of the (linearized) chirality term to the above result, gives the TGB_A interaction energy provided that both $k_0 l \ll 1$ and $k_0 \lambda \ll 1$. If we restrict ourselves to a configuration of straight and nearly parallel screw dislocations, then Eq. (B1) easily reduces to

$$F_{\mathrm{int}}/\Omega = -dh/(l_b l_d) + \frac{K_2}{2} \frac{1}{(2\pi)^3} \int d^3q \frac{|\mathbf{m}(q)|^2}{1 + (\lambda_{\perp 2} q)^2} \ . \tag{B4}$$

Now consider the TGB_A structure with a dislocation configuration given by

$$\mathbf{R}_{kp}(s) = p l_b \hat{\mathbf{x}} + (k l_d + u_{kp}) \hat{\mathbf{e}}_2(p) + s \hat{\mathbf{e}}_1(p) \ . \tag{B5}$$

In this expression $\hat{\mathbf{x}}$,

$$\hat{\mathbf{e}}_1(p) = (0, \cos(p k_1 l_b), \sin(p k_1 l_b))$$

and

$$\hat{\mathbf{e}}_2(p) = (0, -\sin(p k_1 l_b), \cos(p k_1 l_b)) \tag{B6}$$

form a right-hand triad. We also note that the index kp denotes the kth dislocation in the pth grain boundary. Next we define the contribution of the pth grain boundary to the dislocation density

$$\mathbf{m}_p(\mathbf{q}_\perp)\equiv d\sum_k \int ds \frac{d\mathbf{R}_{pk}(s)}{ds} e^{-i\mathbf{q}\cdot\mathbf{R}_{pk}(s)} . \tag{B7}$$

This is related to the previously defined dislocation density $\mathbf{m}(\mathbf{r})=\mathbf{m}(\mathbf{r}_\perp,x)$ via

$$\mathbf{m}(\mathbf{q}_\perp,x)\equiv \sum_p \mathbf{m}_p(\mathbf{q}_\perp)\delta(x-x_p)$$

$$=\int d^2\mathbf{r}_\perp e^{-i\mathbf{q}\cdot\mathbf{r}_\perp}\mathbf{m}(\mathbf{r}_\perp,x) .$$

Reexpressed in terms of $\mathbf{m}_p(\mathbf{q}_\perp)$, Eq. (B4) becomes

$$F_{\rm int}=\frac{K_2}{2\lambda_2^2}\sum_{pp'}\frac{1}{(2\pi)^2}\int d^2q\,\frac{\mathbf{m}_p(q)\cdot\mathbf{m}_{p'}(-q)}{(q^2+\lambda_2^2)^{1/2}} \times\exp[-(q^2+\lambda_2^2)^{1/2}|x_p-x_{p'}|] . \tag{B8}$$

The dislocation interaction energy of the TGB depends on whether the ratio of l_b/P is a rational number or not. If $\alpha=l_b/P_0=P/Q$, a rational number, then the intergrain-boundary terms of Eq. (B8) (i.e., those with $p\neq p'$) will have contributions with nonzero $\mathbf{q}$. These contributions are energies associated with the interdigitation of dislocations in pairs of distant grain boundaries. This weak interdigitation energy can be shown to produce lockin at all rational values of α. Here we shall restrict ourselves to irrational l_b/P_0. In this case

$$\frac{F_{\rm int}}{\Omega}=\frac{K_2}{2l_b\lambda_2}(d/l_d)^2\left[\sum_{n=1}^{\infty}\frac{l_d}{\pi\lambda_2}K_0(nl_d/\lambda_2)+\left[-1+\frac{[1-e^{-l_b/\lambda_2}\cos(k_0l_b)]}{[1-e^{-l_b/\lambda_2}\cos(k_0l_b)]^2+e^{-2l_b/\lambda_2}\sin^2(k_0l_b)}\right]\right] , \tag{B9}$$

where $K_0(x)$ is the Bessel function with an imaginary argument.

In the limit where l_b and $l_d\gg d$, $k_0l_b\ll 1$. If we also suppose l_b and $l_d\gg\lambda_2$, then the TGB free energy simplifies to

$$\frac{F_{\rm TGB}}{\Omega}=\frac{K_2d^2}{2l_bl_d^2\lambda_2}\left[e^{-l_b/\lambda_2}+\left[\frac{l_d}{2\pi\lambda_2}\right]^{1/2}e^{-l_d/\lambda_2}\right]+\frac{\varepsilon_s-hd}{l_bl_d} . \tag{B10}$$

Minimizing the above expression in terms of l_b and l_d, one finds that

$$l_b=\lambda_2\ln\left[\frac{l_b}{l_d}\frac{K_2d}{2(h-h_{c1})\lambda_2^2}\right] ,$$
$$l_d=\lambda_2\ln\left[\frac{l_d}{\lambda_2}\frac{K_2d}{2(h-h_{c1})\lambda_2^2}\right] . \tag{B11}$$

Evidently one obtains a continuous transition in this approximation although it may be difficult for many experiments to distinguish it from a first-order transition. We should also note that Eq. (B11) may be obtained using $k_0\approx d/(l_bl_d)$.

It is also interesting to consider the $\lambda_2\gg\sqrt{l_bl_d}$, limit, where we can expand the right-hand side of Eq. (B8) to obtain

$$\frac{E_{\rm TGB}}{\Omega}\simeq\tfrac{1}{2}K_2d^2\frac{1}{(l_dl_b)^2}+(\varepsilon_s-\mu)/(l_bl_d) . \tag{B12}$$

Let $l\equiv\sqrt{l_bl_d}$. Then Eq. (B12) implies that

$$l=\left[\frac{K_2d}{h-h_{c1}}\right]^{1/2} \tag{B13}$$

and

$$P\simeq\frac{2\pi d}{l_bl_d}=\frac{2\pi K_2}{h-h_{c1}} . \tag{B14}$$

It is unfortunate that the higher-order corrections in l/λ_2, which are required to give the lattice spacing ratio R, are fairly difficult to evaluate. However, preliminary numerical studies indicate that l_b, l_d, and l differ by factors of order unity. Finally we note that Eq. (B11) and (B13) match continuously at $l\sim\lambda_2$.

The above story is modified by several effects that have been ignored. A particularly interesting one is associated with the smectic-layer compressibility [33,34]. It can be included by replacing the smectic-layer spacing d by $d'=d/(1+v)$, where v is a compressional strain, and by adding $\frac{1}{2}B_\parallel v^2$. One may then integrate out the strain to obtain

$$\frac{E_{\rm eff}}{\Omega}=\frac{K_2d^2}{2l_bl_d^2\lambda_2}\left[e^{-l_b/\lambda_2}+\left[\frac{l_d}{2\pi\lambda}\right]^{1/2}e^{-l_d/\lambda}\right]+\frac{\varepsilon_s-hd}{l_bl_d}-\frac{\varepsilon_s^2}{2B_\parallel l_b^2l_d^2} \tag{B15}$$

in the limit where l_b and $l_d\gg\lambda$. This differs from Eq. (B10) by a long-range attractive interaction. The attraction is proportional to $1/l^4$ and, hence, dominates the exponentially screened repulsive interactions. Because of this, the TGB$_A$–Sm-A transition becomes first order. In particular, as $h\to h_{c1}$, l tends to some finite $l_{\max}$ instead of diverging logarithmically. We may get an order of magnitude estimate of $l_{\max}$ by equating the twist repulsion term with the long-range interaction term. One finds that

$$\frac{l_{\max}}{\lambda}=\ln\left[\frac{l_{\max}}{\lambda}\left[\frac{2\pi\lambda}{d}\right]^2\left[\frac{B_\parallel\ln^2\kappa}{B_\perp}\right]\right] . \tag{B16}$$

To get some feeling for the lengths involved, suppose $d=40$ Å and $\lambda=90$ or 185 Å. In these two cases Eq.

(B16) would be $l_{\max}/\lambda_2 = 8.9$ and 7.3, respectively.

A second effect which has been neglected is the long-range entropic repulsion between dislocation lines. Unfortunately, a discussion of thermal fluctuations and the energetics of bent dislocations is well beyond the scope of our discussion. So we will simply note that such a long-range repulsion will tend to make the TGB$_A$–Sm-A transition either second order or more weakly first order.

[1] J. Goodby, M. A. Waugh, S. M. Stein, E. Chin, R. Pindak, and J. S. Patel, Nature **337**, 449 (1988); J. Am. Chem. Soc. **111**, 8119 (1989).

[2] G. Srajer, R. Pindak, M. A. Waugh, J. W. Goodby, and J. S. Patel, Phys. Rev. Lett. **64**, 1545 (1990).

[3] O. D. Lavrentovich, Yu. A. Nishtishin, V. I. Kulishov, Yu. S. Narkevich, A. S. Tolochko, and S. Y. Shiyanovskii, Europhys. Lett. **13**, 313 (1990).

[4] S. R. Renn and T. C. Lubensky, Phys. Rev. A **38**, 2132 (1988).

[5] T. C. Lubensky and S. R. Renn, Phys. Rev. A **41**, 4392 (1990).

[6] P. G. de Gennes, Solid State Commun. **14**, 997 (1973).

[7] S. Fetter and P. Hohenberg, in *Superconductivity,* edited by R. D. Parks (Dekker, New York, 1969).

[8] D. Saint-James, G. Sarma, and E. Thomas, *Type-II Superconductors* (Oxford University Press, New York, 1969).

[9] A. Slaney and J. Goodby, in Proceedings of the 13th International Liquid Crystal Conference, Vancouver, 1990 [Mol. Cryst. Liq. Cryst. (to be published)].

[10] Sm-C^* is a variant of the Sm-C phase which occurs in chiral compounds. Like the Sm-C phase, the director is not parallel to the layer normals but lies at a fixed angle with respect to the layer normal (i.e., the director lies on a cone coaxial with the layer normal). Unlike the Sm-C, the director precesses around this cone as one moves along the layer normal direction. For schematic drawings of the Sm-C and Sm-C^* phases the reader is referred to Ref. [33], pp. 14 and 15.

[11] The first observation that Sm-A is strongly type-II near the Sm-A–Sm-C boundary is due to R. B. Meyer.

[12] J. Goodby and A. Slaney (unpublished).

[13] C. C. Huang, D. S. Lin, J. W. Goodby, M. A. Waugh, S. M. Stein, and E. Chin, Phys. Rev. A **40**, 4153 (1989).

[14] S. R. Renn and T. C. Lubensky, in Proceedings of the 13th International Liquid Crystal Conference, Vancouver, 1990 [Mol. Cryst. Liq. Cryst. (to be published)].

[15] T. C. Lubensky, S. R. Renn, and Tetsuji Tokihiro, in *Quasi-Crystals: The State of the Art,* edited by Paul J. Steinhardt and P. DiVincenzo (World Scientific, Singapore, 1991).

[16] Jing-huei Chen and T. C. Lubensky, Phys. Rev. A **14**, 1202 (1976).

[17] L. J. Martinez-Miranda, A. R. Kortan, and R. J. Birgenau, Phys. Rev. Lett. **56**, 2264 (1986); D. Brisbin, D. L. Johnson, H. Fellner, and M. E. Neubert, *ibid.* **50**, 178 (1983); S. Shashidhar, B. K. Ratna, and S. Krisha Prasad, *ibid.* **53**, 2141 (1984).

[18] N. D. Mermin, D. A. Rabson, D. S. Rokhsar, and D. C. Wright, Rev. Mod. Phys. **41**, 10 498 (1990).

[19] D. A. Rabson, N. D. Mermin, D. S. Rokhsar, and D. C. Wright, Rev. Mod. Phys. **63**, 699 (1991).

[20] J. Toner, Phys. Rev. B **43**, 8289 (1991).

[21] P. G. de Gennes, Solid State Commun. **10**, 753 (1972).

[22] G. Grinstein and R. A. Pelcovits, Phys. Rev. A **26**, 2196 (1982).

[23] T. C. Lubensky, S. Ramaswamy, and J. Toner, Phys. Rev. A **38**, 4284 (1988).

[24] M. Kleman, *Points, Lines, and Walls* (Wiley, New York, 1983).

[25] L. Lejcek, Czech. J. Phys. B **34**, 563 (1984); **35**, 726 (1985).

[26] This definition of the dislocation core differs from that used in previous works by the author. (See Refs. [4, 5] and [14, 15]). In those references, the dislocation core radius was ξ, the smectic coherence length.

[27] A similar phenomenon involving tilt grain boundaries (composed of edge dislocations) has been discussed in S. Ramaswamy and J. Toner (unpublished).

[28] A. Bienenstock and P. P. Ewald, Acta. Crystallogr. **15**, 1253 (1962).

[29] R. Pindak and P. Collings (private communication).

[30] See, for example, P. Bak, Rep. Prog. Phys. **45**, 587 (1981).

[31] M. I. Petrashen and E. D. Trifonov, *Applications of Group Theory in Quantum Mechanics* (MIT, Cambridge, MA, 1969); J. S. Lomont, *Applications of Finite Groups* (Academic, New York, 1959).

[32] A. R. Day, T. C. Lubensky, and A. J. McKane, Phys. Rev. A **27**, 1461 (1983).

[33] P. G. de Gennes, *The Physics of Liquid Crystals* (Oxford University Press, Oxford, 1974).

[34] C. P. Bean and D. S. Rodbell, Phys. Rev. **126**, 104 (1962).